BRILLOUIN SCATTERING EXPERIMENTS ON SINGLE CRYSTALS OF CYCLOHEXANE

SYED FAIZ AHMAD

BRILLOUIN SCATTERING EXPERIMENTS

ON

SINGLE CRYSTALS OF CYCLOHEXANE

by

© Syed Faiz Ahmad, M.Sc. (A.M.U.)

A Thesis submitted in partial fulfillment
of the requirements for the degree of
Master of Science

Department of Physics
Memorial University of Newfoundland

June 1977

St. John's Newfoundland

ABSTRACT

Brillouin scattering experiments were carried out on single crystals of cyclohexane (C_6H_{12}) in the plastic phase, near the triple point, and adiabatic elastic constants were evaluated. Four single crystals were grown in a quartz cell. The crystals were rotated and their orientations with respect to the laboratory frame of reference were determined using X-ray Laue transmission methods. Light (514.5 nm wavelength) from an Ar-ion laser was incident along the vertical axis of the cylindrical cell, and scattering at an angle of 90^{o} was analyzed and recorded by photon counting techniques using a piezoelectrically scanned Fabry-Perot interferometer, photomultiplier tube and a data acquisition and stabilization system.

The spectra usually showed a quasilongitudinal component and a single, very much weaker, quasitransverse component; only three spectra showed both transverse components. By least-squares fitting 59 different frequency shift measurements, the adiabatic elastic constants were determined to be: at 279.2 ± 0.2 K (in units of 10^{9} N m^{-2}),

$$C_{11} = 2.8(57) , \quad C_{12} = 2.4(72) , \quad C_{44} = 0.35(8)$$

with an estimated absolute uncertainty of 2%. This resulted in an adiabatic bulk modulus $B_s = 2.60 \times 10^{9}$ N m^{-2}, and an elastic anisotropy factor A = 1.86.

The results have been compared with those obtained by ultrasonic measurements on polycrystalline samples of C_6H_{12}, with those of other plastic molecular crystals, and also with rare-gas and non-plastic molecular crystals. This is the only experiment where the elastic constants of a plastic crystal of complex molecules have been studied very close to the triple point. It was further established that, even at the triple point, the crystal remained anisotropic.

ACKNOWLEDGEMENTS

I am very grateful to Dr. H. Kiefte and Dr. M. J. Clouter for the suggestion of the problem and their valuable help at every step of this experiment and also in the preparation of this thesis. I am also thankful to Mr. T. White and his staff for their ever willing assistance in the fabrication of the cryostat. My thanks are also due to Mr. R. Guest for the diagrams, and to Miss D. Janes for typing the thesis.

Throughout this research I was supported by a Fellowship and a Teaching Assistantship from Memorial University of Newfoundland which I gratefully acknowledge.

TABLE OF CONTENTS

		Page
ABSTRACT		i
ACKNOWLEDGEMENTS		iii
TABLE OF CONTENTS		iv
LIST OF TABLES		vi
LIST OF FIGURES		vii
CHAPTER 1	INTRODUCTION	1
1.1	Classical Theory of Brillouin Scattering in Cubic Crystals	7
1.2	Propagation of Elastic Waves in Cubic Crystals	16
CHAPTER 2	EXPERIMENTAL APPARATUS	23
2.1	Laser	23
2.2	Spectrometer	26
2.3	Data Acquisition and Stabilization System (DAS)	30
2.4	Sample Cell and Cryostat	32
2.5	Temperature Control and Growth of Single Crystals	38
CHAPTER 3	EXPERIMENTAL ANALYSIS	41
3.1	Orientation of Cubic Crystals by X-Ray Diffraction	41
3.2	Analysis of Spectra	45
3.3	Determination of Elastic Constants	47

		Page
CHAPTER 4	EXPERIMENTAL RESULTS AND DISCUSSION	52
4.1	Orientation of Cyclohexane Crystals	52
4.2	Brillouin Scattering Spectrum of Single Crystals of Cyclohexane	54
4.3	Elastic Constants and Error Analysis	61
4.4	Discussion	65
REFERENCES		73

LIST OF TABLES

		Page
Table 4.1	Physical constants of solid cyclohexane	53
Table 4.2	Observed and calculated Brillouin shifts as a function of orientation for four cyclohexane single crystals, at 279.2 ± 0.2 K	59
Table 4.3	Adiabatic elastic constants of solid cyclohexane at 279.2 ± 0.2 K	62
Table 4.4	Comparative elastic data of some plastic and rare gas crystals	67

LIST OF FIGURES

		Page
Fig. 1.1	Diagram showing the incident wave vector $\vec{k}_o$, the source point $\vec{r}$, the field point $\vec{R}$, and the scattering angle, θ.	8
Fig. 1.2	Scattering of an incident photon. The diagram represents phonon annihilation. The direction of $\vec{K}$ will be reversed in the phonon creation process.	14
Fig. 1.3	Classical Bragg reflection of the incident light wave by elastic waves.	14
Fig. 2.1	Schematic experimental arrangement for Brillouin scattering and X-ray diffraction analysis of cyclohexane single crystals.	24
Fig. 2.2	Schematic diagram of the sample cell and the cryostat. The Fabry-Perot spectrometer axis is perpendicular to the plane of the paper.	34
Fig. 3.1	"Stick-diagram" showing the various measurements made on the spectrum. R's are the Rayleigh components, L's are the longitudinal components and T's the transverse components. Δ, ΔL, and ΔT's are used to calculate the frequency of these components.	46
Fig. 4.1	The transmission Laue photograph of crystal 3 at a particular orientation. Below is shown the computer-plotted Laue pattern and the corresponding Euler angles. The spots are labelled with the Miller indices of the reflecting planes.	55
Fig. 4.2	Brillouin spectrum of crystal 3 at the orientation specified by the Euler angles (θ,ϕ,χ). Only one complete order has been shown. The spectrum was scanned 1575 times at a rate of 2 ms per channel. The incident radiation was polarized perpendicular to the scattering plane.	57

CHAPTER 1

INTRODUCTION

An important landmark in the history of molecular spectroscopy was the revival of Brillouin scattering experiments in the 1960's. After the initial presentation of the theory of light scattering from thermal phonons by Brillouin in 1922 (Russian literature refers to it as the Mandelshtam-Brillouin theory) and the subsequent experimental verification by Gross (1930), not much progress was made in this field. This was mainly because of the severe limitations on the equipment available for high resolution (about 10^8) spectroscopy and the unavailability of highly monochromatic sources. However, working with the available equipment, Krishnan (1955) clearly demonstrated the value of Brillouin scattering as a probe to the dynamical behaviour of solids. The advent of lasers in 1960 provided an ideal light source for Brillouin scattering experiments because of their high monochromaticity, power and directivity. At the same time, refinements in interferometers and detectors were made, thus making it possible to obtain very high resolutions which is essential for Brillouin spectroscopy.

The Brillouin spectrum of light scattered from thermal phonons contains, in its shift, the phase velocity of sound and, in its linewidth, the acoustic absorption. The sound velocities in solids are then used to calculate the elastic constants of a crystal if its orientation is known. Brillouin scattering is now a well-established technique to study gases (see, e.g., Rawson et al. 1966; Greytak and Benedek 1966),

liquids (see, e.g., Chiao and Stoicheff 1964, Fleury and Boon 1969; Clouter et al. 1973, 1975) and solids (see, e.g., Benedek and Fritsch 1966; Shapiro et al. 1966). The theory of light scattering from thermal fluctuations in transparent media is extensively referenced by Rytov (1958) and Fabelinskii (1963, 1968). An excellent introduction to Brillouin scattering in solids and a review of the theory and experiments on solids have been given by Quate et al. (1965), Smith (1971), Cummins and Schoen (1972), and Hayes (1975). Borcherds (1973) gives an introduction to and a simplified theory of Brillouin scattering in cubic crystals, whereas Benedek and Fritsch (1966) and Born and Huang (1954) deal thoroughly with the scattering cross-sections in the same.

A sensitive test of lattice dynamical theories and of the validity of various intermolecular potentials requires an accurate knowledge of the elastic constants. A traditional method for determining elastic constants involves using ultrasonic techniques. If the melting point of a particular crystal material is well above room temperature, it can be cut and oriented and then the acoustic velocities in specific crystal directions can be measured by ultrasonic techniques. This yields quite reliable adiabatic elastic constants, adiabatic modulii and elastic anisotropy. However, at comparatively low triple point temperatures, it is difficult to grow, maintain, cut and orient large crystal specimens, particularly when it is necessary to bond them to ultrasonic transducers. Thus, in such cases, only polycrystalline samples can be used, thereby losing important information regarding the anisotropy and elastic constants of single crystals.

It has already been mentioned that the elastic constants of transparent media, especially at low temperatures, can also be determined by Brillouin spectroscopy. In such experiments, the minimum required scattering volume is about 1 mm^3 and, hence, only small single crystals need to be grown. The crystal need not be physically disturbed either during its growth or in the course of experiment. The crystal orientation can be determined by Laue diffraction photographs. The orientations are readily changed without disturbing the crystal and, hence, velocity as a function of direction can be studied. Also, because of the high resolution and the large signal to noise ratio that can be obtained by using photon counting techniques, the elastic constants, etc., are determined to a high degree of accuracy. Brillouin scattering has been used successfully to determine the adiabatic elastic constants of many types of transparent crystals ranging from diamond (Grimsditch and Ramdas 1975), quartz (Shapiro et al. 1966; Durand and Pine 1968), ionic crystals (see, e.g., Benckert and Backstrom 1973), molecular crystals (see, e.g., Swanson and Dows 1973, 1975), to low temperature rare-gas crystals (see, e.g., Gornall and Stoicheff 1971, Gewurtz et al. 1972), and diatomic gas crystals (see, e.g., Kiefte and Clouter 1975, 1976).

Brillouin spectroscopy up to now has not been used extensively to study molecular crystals which are technologically becoming important materials (Swanson et al. 1975). However, some emphasis has been laid on particular types of molecular crystals called "plastic crystals". Such crystals are formed by cyclohexane, succinonitrile, pivalic acid,

norbornylene, camphine, etc. The word "plastic" was first coined by Timmerman (1953), who surmised the existence of these solids from the anomalous (low) values of the entropies of fusion of organic compounds. He found that globular compounds (i.e., those compounds whose molecules either have a high degree of symmetry about their centres, such as CH_4, or appear to be spherically symmetric because of a rotation about an axis, such as cyclohexane) have low entropies of fusion (< 20 eu), high triple point temperatures and exist in at least two solid phases. The first phase that is formed just below the triple point is usually the plastic crystalline phase. The crystal is clear, tacky and easily deformed, hence the term "plastic". At lower temperatures, this plastic phase transforms into one or two or more non-plastic phases. X-ray studies of this phase indicate structures of high symmetry, usually face or body centered cubic or hexagonal close packed. The X-ray spectra tend to be diffuse and their intensities diminish rapidly with Bragg angle which is evidence of the high degree of molecular disorder (Dunning 1961). NMR and Raman experiments on some of these plastic crystals show that the molecules have a high degree of rotational and translational freedom and that the Raman spectrum is not very significantly different from that of the liquid phase (see, e.g., Mitsuo Ito 1965; Gilbert and Drifford 1977).

Brillouin scattering experiments have been carried out on quite a few compounds showing a plastic phase, viz., succinonitrile (Boyer et al. 1971, Bird et al. 1971), pivalic acid (Bird et al. 1973), norbornylene (Folland et al. 1975), polycrystalline CCl_4 (Levy-Mannheim et al. 1974),

and CBr_4 (Tekippe and Abels 1977). However, only in the case of pivalic acid and norbornylene were the crystal orientations known and the elastic constants and elastic anisotropy calculated.

The ultrasonic measurements (Fontaine and Moriamez 1968) on single crystals of succinonitrile indicated that it is very close to being elastically isotropic; similar observations were made for pivalic acid and norbornylene using Brillouin spectroscopy. The Brillouin scattering experiments by Kiefte and Clouter on γ-oxygen (1975) and β-nitrogen (1976) single crystals at their triple points also indicated that these crystals, especially oxygen, are highly isotropic. Nitrogen and oxygen both exist in the plastic form just below their triple point. Hence, it was suspected that there may be some relationship between the plastic phase of a substance and its elastic isotropy (at least at the triple point). For this reason it was thought necessary to study Brillouin scattering in other plastic crystals, particularly at the triple point, which has not been done in the above mentioned more complex plastic crystals.

One such substance is cyclohexane (C_6H_{12}). It consists of a ring of six carbon atoms to each of which are bonded two hydrogen atoms. The carbon ring is not in a plane as in the benzene molecule but has the 'chair' puckered structure with D_{3d} symmetry (Andrew and Eades 1953, and references cited therein). Cyclohexane forms a plastic crystal phase (phase I) in the temperature range from the triple point* 6.68°C

---

*Physical constants of cyclohexane and their source of references are given in Table 4.1.

(entropy of fusion 9.2 eu) to the first-order phase transition (non-plastic, phase II) at -86°C. In phase I, X-ray investigations (Hassel and Sommerfeldt 1938, Krishna 1958) have shown the crystal lattice to be fcc with four molecules per unit cell, and is confirmed to have space group T_h^2 (Mitsuo Ito 1965).

Previous studies of molecular motion in this plastic phase of cyclohexane have included NMR measurements (Andrew and Eades 1953, Folland et al. 1973), Raman spectroscopy (Mitsuo Ito 1965), infra-red spectroscopy (Carpenter and Halford 1947, Dows 1965) and self-diffusion of vacancies (see, e.g., Hawthorne and Sherwood 1970). Measurements of ultrasonic velocity and absorption have been done by Rasmussen 1962, Gorbunov et al. 1966, Green and Scheie 1967, Koshkin and Dobromyslov 1970, and Dobromyslov et al. 1974). Green and Scheie (1967) have estimated elastic constants of phase I of cyclohexane from their ultrasonic velocity measurements on polycrystalline samples.

In the following pages, some Brillouin scattering experiments on single plastic crystals of cyclohexane very close to the triple point are described. A cryostat was especially designed to grow single crystals and to maintain them for days within 0.1 K temperature variation. The crystal could be rotated about an axis, and the orientations were determined by Laue photographs. The spectrum was recorded at various orientations by Fabry-Perot and photon counting techniques.

In the remaining part of Chapter 1, a brief theory of Brillouin scattering and the propagation of elastic waves in cubic crystals will be presented. In Chapter 2, a description of the apparatus used to grow

crystals, to control the temperature and to record the spectra is given. In Chapter 3, the procedure to analyze the spectra and to calculate the elastic constants is described. The results and error analysis are presented in Chapter 4, which also contains a discussion on these results.

1.1 Classical Theory of Brillouin Scattering in Cubic Crystals

The scattering of light generally arises as the result of optical inhomogeneities in the scattering medium. In homogeneous, pure substances, the reason for optical inhomogeneities has been established as the fluctuation of the optical dielectric constant, brought about in turn by the fluctuations of the density of the substances and fluctuations in the orientation of the molecules.

Using the above arguments, Brillouin scattering in solids has been discussed by many authors (see, e.g., Born and Huang 1954; Benedek and Fritsch 1966, Fabelinskii 1968, and Cummins and Schoen 1972). In this section, the theory developed by Benedek and Fritsch (1966) and later on by Gornall and Stoicheff (1971) is given in brief. This theory predicts the intensity, polarization and frequency of the scattered electromagnetic radiation from a cubic crystal. Only that part of the theory has been discussed which is relevant to this experiment.

There are two basic assumptions made: 1) the solid is regarded as a continuum, and 2) the volume element $|d\vec{r}|$ involved in calculating the scattered electric field is much smaller than the wavelength cubed

of electromagnetic radiation being studied. With these assumptions, the theory proceeds as follows.

An electromagnetic wave passing through a medium produces an oscillating dipole moment per unit volume, $\vec{P}(\vec{r},t)$, at each point $\vec{r}$ (see Fig. 1.1). The scattered or radiated electric field produced by the oscillating $\vec{P}(\vec{r},t)$ in the small volume element $|d\vec{r}|$ is given by

$$d\vec{E}'(\vec{R},t) = \left[\frac{\hat{I}_{R-r} \times [\hat{I}_{R-r} \times \partial^2 \vec{P}(\vec{r},t')/\partial t'^2]}{c^2 |\vec{R}-\vec{r}|} |d\vec{r}| \right]_{t'=t-|R-r|/c_m} , \quad (1.1)$$

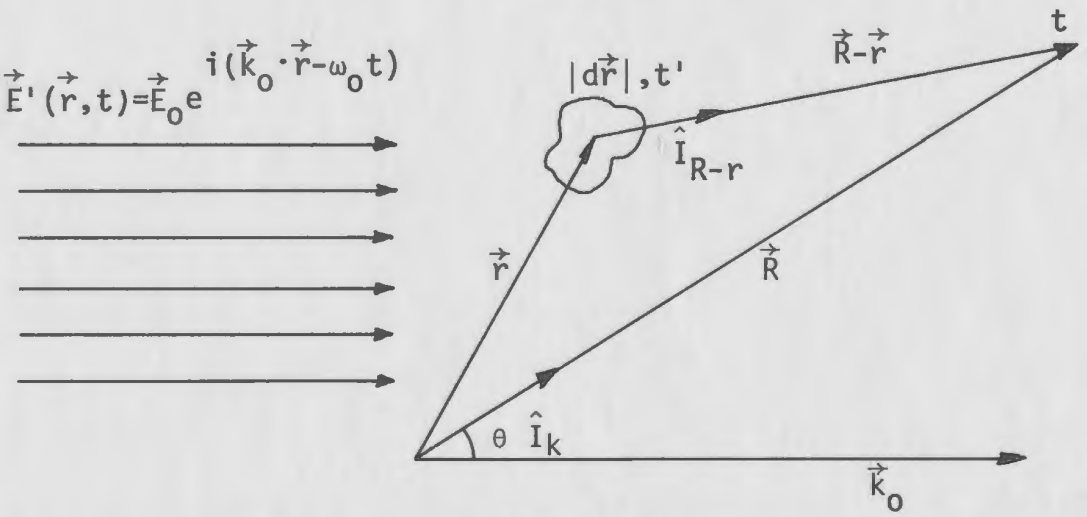

FIGURE 1.1

Diagram showing the incident wave vector $\vec{k}_o$, the source point $\vec{r}$, the field point $\vec{R}$, and the scattering angle θ.

where the vectors are shown in the diagram, $\vec{R}$ being taken inside the scattering medium; t' is the retarded time and $c_m = c/n$ is the velocity of electromagnetic waves in the medium.

Let the electric field of the wave incident within the medium be

$$\vec{E}(\vec{r},t) = \vec{E}_o \, e^{i(\vec{k}_o \cdot \vec{r} - \omega_o t)} \tag{1.2}$$

where the wave vector $|\vec{k}_o| = n\omega_o/c = 2\pi/\lambda_o$, ω_o is the frequency and λ_o is the wavelength of the incident field. The polarization induced by this field can be written as

$$\vec{P}(\vec{r},t) = \left[<\alpha> + \delta\alpha(\vec{r},t) \right] \vec{E}(\vec{r},t) \tag{1.3}$$

where the polarizability tensor α of the medium has been decomposed into the time average part $<\alpha>$, and the time-space fluctuations $\delta\alpha(\vec{r},t)$. Also, α is approximately related to the dielectric constant of the medium as

$$\varepsilon = 1 + 4\pi\alpha \tag{1.4}$$

$$\delta\alpha(\vec{r},t) = \delta\varepsilon(\vec{r},t)/4\pi \quad . \tag{1.5}$$

In liquids and cubic crystals, $<\alpha>$ is a scalar times the unity tensor, and the index of refraction n is independent of direction of propagation. Scattering in the forward direction only is produced by $<\alpha>$, whereas scattering in all other directions arises solely from $\delta\alpha(\vec{r},t)$. The fluctuations in the tensor elements of $\delta\alpha(\vec{r},t)$ are produced because of the density fluctuations which, in turn, are composed of adiabatic fluctuations (thermal pressure fluctuations), and isobaric fluctuations (entropy fluctuations). The pressure fluctuations represent random local compressions or rarefactions which, as a consequence of the elastic properties of the medium, do not remain fixed in position but propagate throughout the volume of the sample. The numerous random

compressions and rarefactions arising from the thermal pressure fluctuations can be considered as elastic waves of different frequencies which are propagated in all possible directions inside the volume under study. These elastic waves have characteristic frequencies $\lesssim 10^3$ GHz which is small compared to the light frequencies in the optical region $\sim 5X10^5$ GHz. Hence, in evaluating $\delta^2\vec{P}/\delta t'^2$, $\delta\alpha$ may be regarded as a very weak function of time. Hence, Eqs. (1.2) and (1.3) give

$$\delta^2\vec{P}(\vec{r},t')/\delta t'^2 \cong - \omega_o^2\vec{P}(\vec{r},t') \quad . \tag{1.6}$$

Substituting Eqs. (1.6), (1.3) and (1.2) in (1.1) and taking into account the time retardation, the following expression is obtained.

$$d\vec{E}'(\vec{R},t) = - (\omega_o/c)^2 \frac{\hat{I}_{R-r}}{|\vec{R}-\vec{r}|}$$

$$X \left[\hat{I}_{R-r} X \{(<\alpha> + \delta\alpha(\vec{r},t')) \vec{E}_o e^{i\vec{k}_o\cdot\vec{r}} e^{i\omega_o(\frac{n}{c}|\vec{R}-\vec{r}|-t)} \} |d\vec{r}| \right] \tag{1.7}$$

If $R >> r$, then the following assumptions can be made:

$$\hat{I}_{R-r} \cong \hat{I}_k \; ; \quad |\vec{R}-\vec{r}| \simeq R$$

$$\frac{n\omega_o}{c}|\vec{R}-\vec{r}| \cong \frac{n\omega_o}{c}\hat{I}_k\cdot(\vec{R}-\vec{r}) = \vec{k}'_o\cdot(\vec{R}-\vec{r})$$

$$\vec{k}'_o \equiv \frac{n\omega_o}{c}\hat{I}_k$$

and carrying out the integration over the illuminated volume v at the retarded time t' to get

$$\vec{E}'(\vec{R},t) = -\left(\frac{\omega_o}{c}\right)^2 \frac{e^{i(\vec{k}_o'\cdot\vec{R}-\omega_o t)}}{R} \hat{I}_k \times \left[\hat{I}_k \times \int_v \{<\alpha> + \delta\alpha(\vec{r},t')\} \cdot \vec{E}_o \, e^{i(\vec{k}_o-\vec{k}_o')\cdot\vec{r}} \, |d\vec{r}|\right] . \qquad (1.8)$$

It can be seen right away that the contribution by the $<\alpha>$ term is only in the forward direction because of the Dirac delta function. Hence, in this case where $\vec{k}_o \neq \vec{k}_o'$,

$$\vec{E}'(\vec{R},t) = -\left(\frac{\omega_o}{c}\right)^2 \frac{e^{i(\vec{k}_o'\cdot\vec{R}-\omega_o t)}}{R} \hat{I}_k \times \left[\hat{I}_k \times \int_v \{\delta\alpha(\vec{r},t')\cdot\vec{E}_o\} \cdot e^{i(\vec{k}_o-\vec{k}_o')\cdot\vec{r}} \, |d\vec{r}|\right] . \qquad (1.9)$$

It has already been stated that the fluctuations in the medium take place in all the directions. However, only particular fluctuations are responsible for scattering in a particular direction. In order to find that, the fluctuations are analyzed into their spatial Fourier components:

$$\delta\alpha(\vec{r},t') = (2\pi)^{-3/2} \sum_\mu \int |d\vec{q}| \; \delta\alpha^\mu(\vec{q}) \, e^{i(\vec{q}\cdot\vec{r} \mp \omega_\mu(\vec{q})t')} \qquad (1.10)$$

where $|\vec{q}| = 2\pi/\lambda$ is the wave vector of the fluctuation and $\omega_\mu(\vec{q})$ is the frequency corresponding to this fluctuation. The index μ denotes the possibility of a number of branches in the dispersion relation connecting

$\vec{q}$ and ω. The double value ($\pm$) of $\omega_\mu(\vec{q})$ is taken into account for waves in opposite directions.

Eq. (1.10) is substituted into (1.9) and the retarded time is eliminated to obtain:

$$\vec{E}'(\vec{R},t) = -\left(\frac{\omega_o}{c}\right)^2 \sum_\mu \hat{I}_k \times \left\{ \hat{I}_k \times \int |d\vec{r}| \int |d\vec{q}| \; \{\delta\alpha(\vec{q})\cdot\vec{E}_o\} \frac{e^{i(\vec{k}_o'\cdot\vec{R}-\omega_o t)}}{(2\pi)^{3/2} R} \right.$$

$$\left. \cdot\, e^{i(\vec{k}_o-\vec{k}_o')\cdot\vec{r}}\, e^{i\vec{q}\cdot\vec{r}}\, e^{\mp i\omega_\mu(\vec{q})\left(t - \frac{\vec{R}-\vec{r}}{c} n\right)} \right\} . \qquad (1.11)$$

Letting $$\vec{k} = (n/c)\{\omega_o \pm \omega_\mu(\vec{q})\}\, \hat{I}_k = \vec{k}(\vec{q}) \qquad (1.12)$$

$$\vec{E}'(\vec{R},t) = -\left(\frac{\omega_o}{c}\right)^2 \sum_\mu \hat{I}_k \times \left\{ \hat{I}_k \times \int |d\vec{q}| \; \{\delta\alpha(\vec{q})\cdot\vec{E}_o\} \frac{e^{i(\vec{k}\cdot\vec{R}-\{\omega_o \pm \omega_\mu(\vec{q})\}t)}}{R} \right.$$

$$\left. \cdot\, \{(2\pi)^{-3/2} \int |d\vec{r}|\; e^{i(\vec{k}_o-\vec{k}+\vec{q})\cdot\vec{r}} \} \right\} . \qquad (1.13)$$

The last integration is a Dirac delta function

$$\int |d\vec{r}|\; e^{i(\vec{k}_o-\vec{k}+\vec{q})\cdot\vec{r}} = (2\pi)^3\, \delta\{\vec{q}-(\vec{k}-\vec{k}_o)\} \quad . \qquad (1.14)$$

Thus, unless the relation

$$\vec{q} = \vec{k}-\vec{k}_o \equiv \vec{K} \qquad (1.15)$$

is satisfied, $\vec{E}'$ will be zero and there will be no scattering. $\vec{K}$ is called the scattering vector. This means that the fluctuations which give

rise to scattering in the $\hat{I}_k$ direction must have wave vector $\vec{q} \equiv \vec{K}$, which satisfies the implicit Eq. (1.15).

Eq. (1.5) is substituted into Eq. (1.13) and, emphasizing the dependence of the scattered field on the direction of scattering by relabelling $\vec{E}'(\vec{R},t) = \vec{E}'(\vec{K},t)$,,

$$\vec{E}'(\vec{K},t) = -\left(\frac{\omega_o}{c}\right)^2 \frac{(2\pi)^{3/2}}{4\pi R} \sum_{\mu} e^{i(\vec{k}\cdot\vec{R}-\{\omega_o \pm \omega_\mu(\vec{K})\}t)}$$

$$\cdot \hat{I}_k \times \left(\hat{I}_k \times \{\delta\varepsilon^\mu(\vec{K})\cdot\vec{E}_o\}\right) . \qquad (1.16)$$

Thus it can be seen that the amplitude of the scattering from each branch μ is proportional to that spatial Fourier component of the fluctuation in ε which has wave vector $\vec{K}$. The frequency of the scattered wave is given by

$$\omega = \omega_o \pm \omega_\mu(\vec{K}) \quad . \qquad (1.17)$$

Hence, the spectrum of the scattered light contains sets of doublets located symmetrically around the incident light frequency.

The physical interpretation of Eqs. (1.15) and (1.17) can be described in two ways:

1) In quantum mechanical language, the incident radiation consists of photons of energy $\hbar\omega_o$ and momentum $\hbar\vec{k}_o$. The elastic waves consist of phonons of energy $\hbar\omega_\mu$ and momentum $\hbar\vec{K}$. In the scattering process depicted by Fig. 1.2, the incident photon either creates a phonon or annihilates a phonon at the scattering point. The conservation of

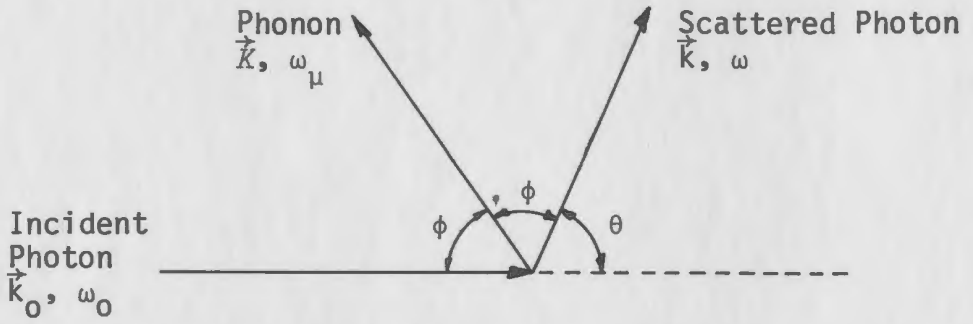

FIGURE 1.2

Scattering of an incident photon. The diagram represents phonon annihilation. The direction of $\vec{K}$ will be reversed in the phonon creation process.

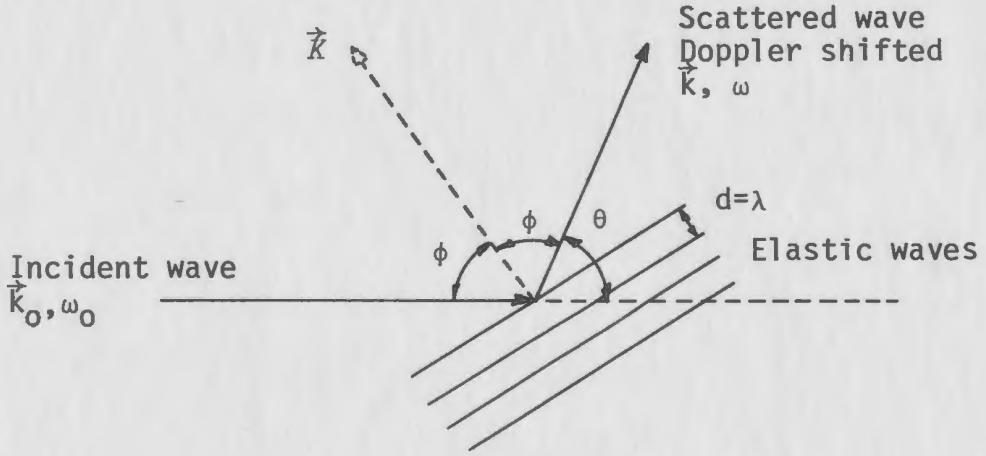

FIGURE 1.3

Classical Bragg reflection of the incident light wave by elastic waves.

momentum and energy then lead to the conditions that the scattered photon has momentum

$$\hbar\vec{k} = \hbar\vec{k}_o \pm \hbar\vec{K} \tag{1.18}$$

and energy

$$\hbar\omega = \hbar\omega_o \pm \hbar\omega_\mu \quad . \tag{1.19}$$

The doublets observed in the spectrum thus represent the exchange of energy $\pm\hbar\omega_\mu$ between the photon and the phonon. Eqs. (1.18) and (1.19) are identical to Eqs. (1.15) and (1.17).

2) In classical mechanics, Eq. (1.14) determines the manner in which the phases of waves scattered from each point of the small scattering volume add up. If the phases add up in accordance with the condition of Eq. (1.15), the scattered radiation adds constructively at each point. This corresponds to a Bragg reflection of the light waves of wavelength λ_o off the wavefronts of the fluctuation of wavelength λ=d, as shown in Fig. 1.3, satisfying the condition

$$\begin{aligned} \lambda_o &= 2\lambda \cos\phi \\ &= 2\lambda \sin\theta/2 \end{aligned} \tag{1.20}$$

where only one order is observed. Since the acoustic waves are travelling with velocity

$$v_\mu(\vec{K}) = \pm \frac{\omega_\mu(\vec{K})}{|\vec{K}|} \quad , \tag{1.21}$$

the wave fronts act like "moving mirrors" and the scattered wave undergoes a Doppler shift which is given by

$$\Delta\omega = \pm 2n\omega_o(v_\mu/c) \sin(\theta/2) \quad . \tag{1.22}$$

From Eqs. (1.15) and (1.17), it can be shown that the Brillouin shifts in the scattered light are exactly equal to the Doppler shifts. Thus,

$$\omega_\mu = \omega_o \mp \omega = \Delta\omega \quad . \tag{1.23}$$

However, neither of the two interpretations mentioned above takes into account the finite lifetime of the sound waves in the medium which results in the broadening of the Brillouin components. This is taken into account by the theory presented by Benedek and Fritsch (1966).

If the frequency shift of the Brillouin components is measured, then, according to Eq. (1.22), the angular dependence of the velocity of these sound waves in the crystal can be determined. In the next section it will be seen that some very important properties of the crystal medium, such as the adiabatic elastic constants and the adiabatic bulk modulus of the cubic crystals, can also be calculated.

1.2 Propagation of Elastic Waves in Cubic Crystals

It has already been pointed out that the Brillouin scattering arises from the thermal fluctuations in the crystal. These fluctuations are, in fact, the thermally-excited elastic waves which are caused by the fluctuations of the strain tensor defined as

$$e_{kl} = \frac{\partial u_k}{\partial r_l} \tag{1.24}$$

where $\vec{u}$ and $\vec{r}$ are the displacement and position vectors of a volume element in the sample.

The generalized Hooke's law states that the components of stress, T_{ij}, at any point of a body are a linear function of the components of the strain at the point. This is written as

$$T_{ij} = C_{ijkl}\, e_{kl} \; ; \quad i, j, k, l = 1, 2 \text{ or } 3 \; . \tag{1.25}$$

The C's are the elastic stiffness constants (usually referred to as elastic constants), and the indices refer to the three orthogonal directions corresponding to the coordinate axes which coincide with the edges of the cubic crystal. The stress components are defined as

$$T_{ij} = \lim_{\Delta A_j \to 0} \left(\frac{\Delta F_i}{\Delta A_j} \right) \tag{1.26}$$

where ΔF_i is the force acting in the i-direction across the element of surface ΔA_j whose normal is in the j-direction.

In general, Eq. (1.25) represents nine equations involving 81 elastic constants. However, by applying the condition that the total torque on the cubic solid should be zero, the number of stress and strain components reduce to six each and the elastic constants to 36. Consideration of the elastic energy density of the crystal further reduces the number of elastic constants to 21. Again, the inherent symmetry of a cubic

crystal (Kittel 1971) reduces the number of independent elastic constants to three. In the light of the above discussion, the stress components are symmetrical, i.e.,

$$T_{ij} = T_{ji} \tag{1.27}$$

and the symmetrized strains are then defined as

$$e_{ij} = \frac{1}{2}\left(\frac{\partial u_i}{\partial r_j} + \frac{\partial u_j}{\partial r_i}\right) \quad . \tag{1.28}$$

For convenience, Eq. (1.25) is written as

$$T_i = C_{ij}\, e_j \tag{1.29}$$

where the tensor notation has been replaced by the matrix notation as follows:

$11 \rightarrow 1$	$23 \rightarrow 4$
$22 \rightarrow 2$	$13 \rightarrow 5$
$33 \rightarrow 3$	$12 \rightarrow 6$.

For the cubic crystals, the matrix C_{ij} is of the form (Kittel 1971),

$$|C_{ij}| = \begin{vmatrix} C_{11} & C_{12} & C_{12} & 0 & 0 & 0 \\ C_{12} & C_{11} & C_{12} & 0 & 0 & 0 \\ C_{12} & C_{12} & C_{11} & 0 & 0 & 0 \\ 0 & 0 & 0 & C_{44} & 0 & 0 \\ 0 & 0 & 0 & 0 & C_{44} & 0 \\ 0 & 0 & 0 & 0 & 0 & C_{44} \end{vmatrix} \tag{1.30}$$

where C_{11} is the longitudinal modulus along a cube edge, C_{44} is a transverse (shear) and $(C_{11}-C_{12})/2$ represents a second transverse modulus. The elastic energy density given by

$$U = C_{ij}\, e_i\, e_j/2 \tag{1.31}$$

must be positive for the crystal to be stable. This implies that

$$C_{44} > 0\ , \qquad C_{11} > |C_{12}|\ , \qquad C_{11} + 2C_{12} > 0\ .$$

In general, a cubic crystal may not be elastically isotropic and the anisotropy factor is given by

$$A = 2C_{44}/(C_{11} - C_{12})\ . \tag{1.32}$$

$A = 1$ for an isotropic cubic crystal.

The adiabatic bulk modulus (the reciprocal of volume compressibility) is given by

$$B = V\left(\frac{\partial P}{\partial V}\right)_T = \frac{1}{3}\,(C_{11} + 2C_{12}) \tag{1.33}$$

where V is the volume, T the temperature, and P is the pressure of the solid.

If we consider the forces acting on a unit volume of the solid, we can apply Newton's second law to obtain the equations of motion in the r_i-direction as

$$\rho\,\frac{d^2u_i}{dt^2} = \frac{dT_{ij}}{dr_i} \tag{1.34}$$

where ρ is the density of the medium. If the heat exchange during a period of oscillatory motion is negligible (as is the case in the Brillouin scattering experiment), then any part of the body is thermally isolated and the deformation is adiabatic; thus all the corresponding observations are adiabatic.

Considering Eqs. (1.28), (1.29), (1.30), and (1.34), the equation of motion in the r_1-direction becomes

$$\rho\frac{d^2u_1}{dt^2} = C_{11}\frac{d^2u_1}{dr_1^2} + C_{44}\left[\frac{d^2u_1}{dr_2^2} + \frac{d^2u_1}{dr_3^2}\right] + (C_{12} + C_{44})\left[\frac{d^2u_1}{dr_1dr_2} + \frac{d^2u_1}{dr_1dr_3}\right]. \quad (1.35)$$

Similar equations exist for motion in the r_2- and r_3-directions. These are obtained by the cyclic permutation of u's and r's.

For the case of a monochromatic plane elastic wave, the solution is of the form

$$\vec{u}(\vec{r},t) = u_o(\vec{q})\ \hat{\Pi}\ (\hat{q})\ e^{i(\vec{q}\cdot\vec{r}-\omega t)} \quad (1.36)$$

where u_o is the magnitude of the particle amplitude and $\hat{\Pi}(\hat{q})$ is the unit vector in the direction of particle motion or, in other words, is the unit polarization vector of the plane wave. Eq. (1.35) can be written as

$$(\lambda_{ij} - \rho\omega^2\delta_{ij})\ \hat{\Pi}_j = 0 \quad (1.37)$$

where
$$\lambda_{ij} = (C_{11} - C_{44})q_i^2 + C_{44}\ q^2 \qquad \text{for } i = j$$
$$= (C_{12} + C_{44})q_iq_j \qquad \text{for } i \neq j\ . \quad (1.38)$$

The system of Eqs. (1.37) is a 3X3 eigenvalue problem. It can be solved by Jacobi's method which involves finding the orthogonal transformation that diagonalizes the matrix λ_{ij}. The three eigenvalues M_μ so obtained yield

$$\omega_\mu(\vec{q}) = \pm (M_\mu/\rho)^{1/2} \qquad \mu = 1,2,3 \qquad (1.39)$$

and the columns of the transformation matrix (the eigenfunctions) are the required unit polarization vectors $\hat{\Pi}^\mu(\hat{q})$. Because λ is symmetric, the three $\hat{\Pi}^\mu(\hat{q})$ for a given $\vec{q}$ are mutually orthogonal. From the dispersion relation

$$\vec{V}_\mu(\vec{q}) = \omega_\mu(\vec{q})/\vec{q} \qquad (1.40)$$

and from Eq. (1.38), it can be seen that, since λ is quadratic in q, the polarizations $\hat{\Pi}^\mu(\hat{q})$ and the velocities $\vec{V}_\mu(\vec{q})$ are dependent only on the direction of $\vec{q}$ and not on its magnitude.

For example, if $\vec{q}$ is parallel to one of the high symmetry directions <100>, <110> or <111>, the highest velocity mode is purely longitudinal (i.e., say, $\hat{\Pi}^1(\hat{q})$ parallel to $\vec{q}$), while the other two modes are transverse and degenerate for propagation in the <100> and <111> directions (i.e., $\omega_2(\vec{q}) = \omega_3(\vec{q})$). In general, however, for an arbitrary direction in an anisotropic cubic crystal, all three modes are non-degenerate; the polarizations are neither strictly longitudinal nor strictly transverse.

Now, in the laboratory frame of reference, the directions of $\vec{k}$ and $\vec{k}_o$ are known and the direction of $\vec{K}$ is known through Eq. (1.15). However, in order to use $\omega_\mu(\vec{K})$, which are the observed Brillouin shifts,

to determine the elastic constants, the direction of $\vec{K}$ must be known in the crystal reference frame. Once this is done as described in Section 3.3, the observed acoustic frequencies are used to determine the adiabatic elastic constants of the crystal.

CHAPTER 2

EXPERIMENTAL APPARATUS

The experimental arrangement for Brillouin scattering studies and also for X-ray diffraction analysis of cyclohexane single crystals is shown in Fig. 2.1. The crystals were grown in a specially designed cryostat. Once a crystal was formed, a transmission Laue photograph was taken to find its orientation with respect to the laboratory frame of reference. Light from a single mode Argon-ion laser was incident along the vertical axis of the sample cell, and Brillouin scattering at 90^{o} was analyzed by means of a piezo-electrically scanned Fabry-Perot interferometer and a photomultiplier tube. The spectrum was stored in a data acquisition and stabilization system. Details of the equipment are given in the following sections.

2.1 Laser

One of the stringent requirements for Brillouin spectroscopy is that the incident radiation should be highly monochromatic. This is because the magnitude of the frequency shifts observed is about 0.1 to 10 GHz and, if the linewidth of the incident radiation is comparable to these shifts, they will not be resolved. The invention of laser provided a highly monochromatic source to be used in such studies.

The source of incident radiation used was an Argon-ion laser (Model 52, Coherent Radiation Labs.). It essentially consists of a high-current gas discharge tube, excited with a direct current of about 20 A

FIGURE 2.1

Schematic experimental arrangement for Brillouin scattering and X-ray diffraction analysis of cyclohexane single crystals.

LASER	Single-mode Argon-ion laser
BS	Beam steerer
Y AXIS	Optic axis - direction of observation
XR	X-ray source
CO	Collimator
L1,2,3,4	Lenses
M	Mirror
Z AXIS	Incident beam direction
CR	Cryostat
PC	Polaroid camera
A1,2	Apertures
FP	Fabry-Perot interferometer
PMT	Cooled photomultiplier tube
AD	Amplifier/discriminator
DAS-1	Data Acquisition and Stabilization System
REC	Chart recorder
TC	Thermoelectric cooling
TMC	Temperature measurement and control

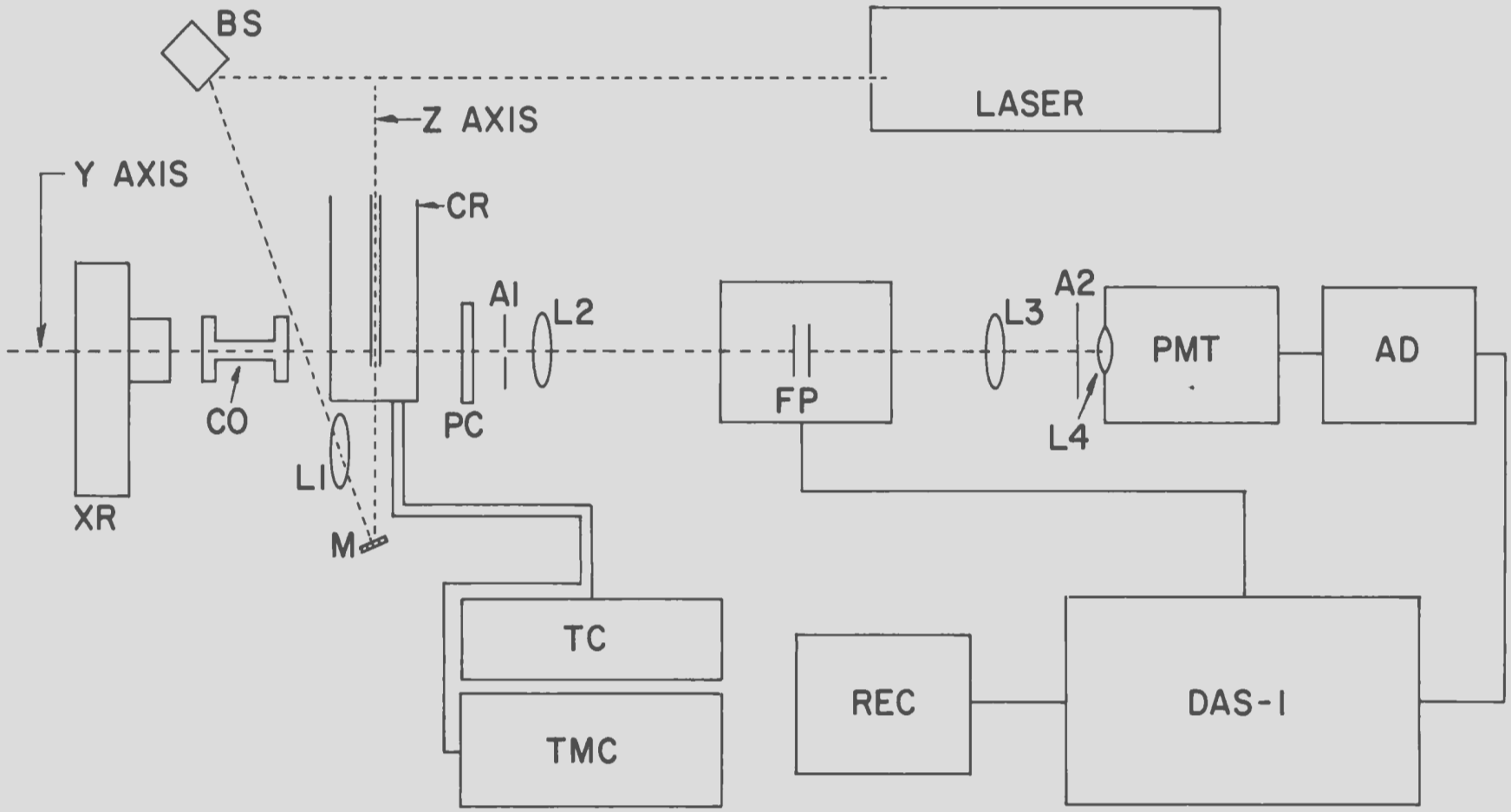
BS
LASER
Z AXIS
Y AXIS
CR
A1
L2
L3
A2
PMT
AD
CO
PC
FP
L4
L1
XR
M
TC
TMC
REC
DAS-1

FIGURE 2.1

and placed in an optical cavity of 1.18 m in length. Its principal emission (of about 2 watts) is in the blue-green region of the visible spectrum, and one particular laser line at 514.5 nm was selected by the use of an intracavity prism (Model 431, Coherent Radiation). This line has a Doppler broadened width of a few GHz, the axial mode spacing within the Doppler profile being $\sim$ 115 MHz. In addition, by using an intracavity etalon (Coherent Radiation), laser action was restricted to one mode. It was observed that, during the first few hours the laser was on, it changed modes ("mode hopped") quite frequently but, after an initial warm-up of several hours, mode hopping was about once every two to three hours. No further attempts at stabilizing the laser were made in these experiments. The laser line had a width of about 20 MHz due to high frequency "jitter". For a detailed description of the laser and Fabry-Perot interferometer used in this laboratory, the reader is referred to the M.Sc. thesis by Morgan (1976).

2.2 Spectrometer

The laser beam, with an average power of 30 mW and always polarized perpendicular to the scattering plane, was directed into the sample cell by means of a beam-steering device (Model BA 500A, Jodon Engineering Assoc., Inc.). It was brought to a focus about 4 mm above the bottom clip of the cell by a 25-cm focal length high quality quartz lens (L1). The light scattered through 90^{o} from the focus was collected through an aperture (A1) of approximately 6 mm diameter and then collimated by a lens (L2) of focal length 40 cm before entering the Fabry-Perot interferometer.

The Brillouin scattering technique involves measurements of very small frequency shifts of the order of 10^{-4} to 10^{-6} of the incident frequency. This necessitates the use of a high resolving power spectrometer which, in the present experiments, consisted of a Fabry-Perot interferometer (RC-40, Burleigh) and a photomultiplier tube.

A Fabry-Perot interferometer (FP) consists of two partially transmitting mirrors (flat or curved) parallel to each other. If the cavity between the two mirrors is illuminated with a beam of coherent, monochromatic light, it will transmit the beam only when the relation

$$m\lambda = 2nd \cos \theta \qquad (2.1)$$

is satisfied, where

λ = wavelength of the incident light

m = order of interference

n = refractive index of the medium between the two mirrors

d = mirror spacing

θ = inclination of the normal of the mirrors to the wavefront direction.

However, only the light transmitted along the optical axis for which $\theta \approx 0$ was studied. This is called central spot scanning, and the Eq. (2.1) reduces to

$$m\lambda = 2d \qquad (n=1, \text{ for air}) \ . \qquad (2.2)$$

Thus, if d is varied, then the wavelength and the order of the transmitted light will change. Tuning is accomplished by moving one mirror with

respect to the other and this is done by using piezoelectric (PZT) crystals. To a good approximation, the plate separation d varies linearly with the voltage applied to the PZT's. The spectrum of the light is obtained by sweeping the voltage while observing the intensity at the center of the ring pattern. The Data Acquisition and Stabilization system (DAS, to be described in Section 2.3) provided totally automatic control of the FP alignment. The interference pattern of the FP was focussed on to a pinhole of 800 μ diameter by means of a 59.1 cm focal length quartz lens (L3). The light from the pinhole was again focussed by another lens of focal length 7 cm on to the cathode of a photomultiplier tube.

The frequency interval between the two consecutive orders of the FP is called the Spectral Free Range (SFR), and is given by

$$SFR = c/2nd \qquad (Hz) \qquad (2.3)$$

where c is the velocity of light in vacuum. For some of the experiments, d was 0.7605 ± 0.0005 cm which gave a SFR of 19.71 ± 0.01 GHz. In the other experiments, d was 0.8011 ± 0.0005 cm which corresponds to a SFR of 18.72 ± 0.01 GHz, and was determined using a travelling microscope.

The instrumental linewidth (full width at half maximum intensity) is given by

$$\Delta\nu = SFR/F \qquad (2.4)$$

where F is the finesse of the Fabry-Perot interferometer. Thus, the finesse is the key measure of the interferometer's ability to resolve closely-spaced lines. F is determined by

$$F^{-2} = F_R^{-2} + F_F^{-2} + F_D^{-2} + F_P^{-2} \qquad (2.5)$$

where F_R, F_F, F_D, and F_P are the contributions due to the mirror reflectivity, mirror flatness, diffraction at the pinhole, and the pinhole size, respectively. The mirrors used in this experiment were 5.08 cm diameter with $\lambda/200$ flatness and dielectrically coated for a reflectivity of 98% at λ = 500 nm. The diameter of the pinhole aperture A2 used was 800 microns.

The various finesse contributions were then calculated* as

$$F_R = 160 \qquad F_F = 100$$

$$F_D = 340 \qquad F_P = 140$$

and, thus, $F \sim 70$.

Hence, the overall instrumental line width was approximately 280 MHz for all the experiments as verified by measurement.

The photomultiplier tube used was an ITT FW130 (Electro-Optical Products Div. ITT). This is a special purpose 16-stage multiplier phototube having a circular end-window photocathode of 2.5 mm diameter. The tube was mounted in a thermoelectrically-cooled, RF-shielded chamber (Model TE104RF, Product for Research), which controlled the cathode temperature to $-20^{o}C \pm 0.5^{o}C$ and had the effect of limiting the dark count to a very low value of about 1 per second.

---

*(Burleigh, Tech. Memo for Fabry-Perot Interferometer)

The output pulses from the phototube were amplified by an Amplifier/Discriminator (AD) (Model SSR 1120, Princeton Applied Research). The unit was installed close to the phototube so that the very weak photopulses were not appreciably attenuated and noise pickup was reduced. The output from the AD was connected to the scalar of the DAS system.

2.3 Data Acquisition and Stabilization System (DAS)

The DAS-1 (Burleigh Instruments Inc.) system was designed for repetitive scanning of the FP and for photon counting detection. In addition, it also automatically corrects for frequency drifts in the entire system as well as for misalignment of the FP cavity.

DAS-1 consists of a multichannel analyzer of 1024 channels. It generates a digital ramp voltage which is used to drive the PZT's of the FP through a high voltage amplifier module. The same ramp voltage also sequentially addresses the 1024 channels. The optical frequency passed by the interferometer varies linearly with the ramp voltage and thus with the channel number. Each time a photopulse arrives, a count is added to the memory channel corresponding to that section of the ramp voltage and, therefore, frequency shift. The photopulses are thus counted and stored and, hence, result in the accumulation of the frequency spectrum of the scattered light in the memory. Logic circuitry prohibits data acquisition during the fly-back portion of the ramp waveform.

The spectrum can be seen on the CRT display of the DAS-1 system. The "Bug" is an intensified spot on the CRT which can be

positioned to address any channel of the memory. The alphanumeric readout on the CRT displays the Bug channel number, the total number of counts in that channel, full scale of the CRT display, and also the total number of scans completed if the Bug is in channel zero. The spectrum display can be linear or logarithmic. An additional facility for background subtraction is also provided.

The effect of long-term frequency drift of the laser, axial drift of the interferometer cavity, or any other possible drift and instability, is eliminated by the drift stabilization unit of DAS-1. This is done by locking the Rayleigh line of the Brillouin spectrum to an arbitrarily defined position in the DAS-1 memory. The stabilizer uses two data windows that are symmetrically located with respect to the Rayleigh line. The center position and the window width is selected by the Bug, and vertical markers clearly indicate the window positions. Suppose the center position is at channel #N, and the width of the windows is ΔN channels. Then during each sweep by the ramp, a register A keeps a running total of the photon counts falling in the lower window, channels $N-\Delta N$ to $N-1$, while a second register B records a similar total for the upper window, channels $N+1$ to $N+\Delta N$. If the number of counts, say, in A are more than in B (taking into account statistical fluctuations), this indicates the shift of peak towards A. During the fly-back time of the sweep, the stabilizer compares the contents of A and B, resets each to zero, and applies a small correction to the bias so as to shift the center of the spectral feature closer to the center of the selected position in the DAS-1 memory. The magnitude of

correction applied per sweep is adjustable by a factor of 16:1 in steps of 2x. The appropriate value is adjusted manually by observing the drift rate and the sweep rate which was normally 2 ms/ch.

Using a method essentially similar to the above, finesse optimization is achieved. In two narrower finesse windows which are centered on the same chosen spectral feature as above, counts are accumulated on each sweep. On every second sweep, small test voltages are applied to the PZT elements to tilt the mirrors first in a direction about the vertical axis. Counts are compared in the third sweep and a correction voltage is applied to maximize the counts. Again in the fourth sweep a test voltage is applied to tilt the mirrors about the horizontal axis. The total counts are compared in the two consecutive sweeps and a small correction voltage (compared to the test voltage) is applied to the PZT elements to tilt the mirrors in the direction corresponding to a greater number of counts, i.e., higher finesse. The magnitudes of test voltage and the correction voltage are adjustable manually.

To record the spectra permanently, the output from the DAS-1 is fed into a strip-chart recorder (Model 7133A Recorder, Hewlett-Packard).

2.4 Sample Cell and Cryostat

A schematic diagram of the sample cell and the cryostat is shown in Fig. 2.2. The basic consideration in designing the cryostat for growing single crystals was to make it as simple and effective as

possible. It was decided to avoid the sophistication available in commercial low-temperature cryostats and the use of cryogens which was unnecessary for the relatively high temperatures in the present work.

The sample cell was a quartz tube of inner diameter 3 mm, 1 mm thick walls and 50 cm long. This tube was rigorously and painstakingly cleaned of dust and impurities with inorganic and organic solvents. The final washing was done with spectroscopic grade methanol. The lower end of the cell was closed with a cylindrical quartz window (W1) which was 5 mm in length. This window was cemented to the cell by means of epoxy. The two faces of the window were highly polished so as to minimize parasitic scattering.

Liquid cyclohexane (Baker Instra-Analyzed, GB Spectrophotometric Grade for crystals #1 and #2; and Anachemia, U.V. Spectrophotometric Grade for crystals #3 and #4), was admitted to the cell by means of a syringe. No special precautions were taken to store the cyclohexane samples and no attempts were made to further purify them. The tube was filled with cyclohexane to a height of about 15 cm. Half the tube was then dipped in liquid nitrogen to freeze the cyclohexane, while the open end of the tube was connected to a vacuum pump which removed the air from the cell. The cell was then slowly warmed and the procedure was repeated, thereby removing most of the dissolved oxygen and nitrogen (which, e.g., are known to have created an error in the measurement of the melting point of C_6H_{12} (Stokes and Tomlins 1974)). While maintaining the vacuum, the top part of the cell was then sealed by melting the quartz.

FIGURE 2.2

Schematic diagram of the sample cell and the cryostat. The FP spectrometer axis is perpendicular to the plane of the paper.

QT	Quartz tube
EC	Electrical connections
VP	Vacuum pump
PTC,PBC	Plexiglass top and bottom covers
BB	Ball bearings
PS	Plexiglass spacer
BC	Brass clips
TC	Thermocouple
DI	Diode
W1,W2	Fused quartz windows
Z	Direction of incident laser beam
OR	Rubber O-ring
HS	Heat sink
TM	Thermoelectric module
CB	Copper braids
HW	Heater wires
CR	Copper rod
PT	Plexiglass tube
ARC	Arrangement for rotating the cryostat

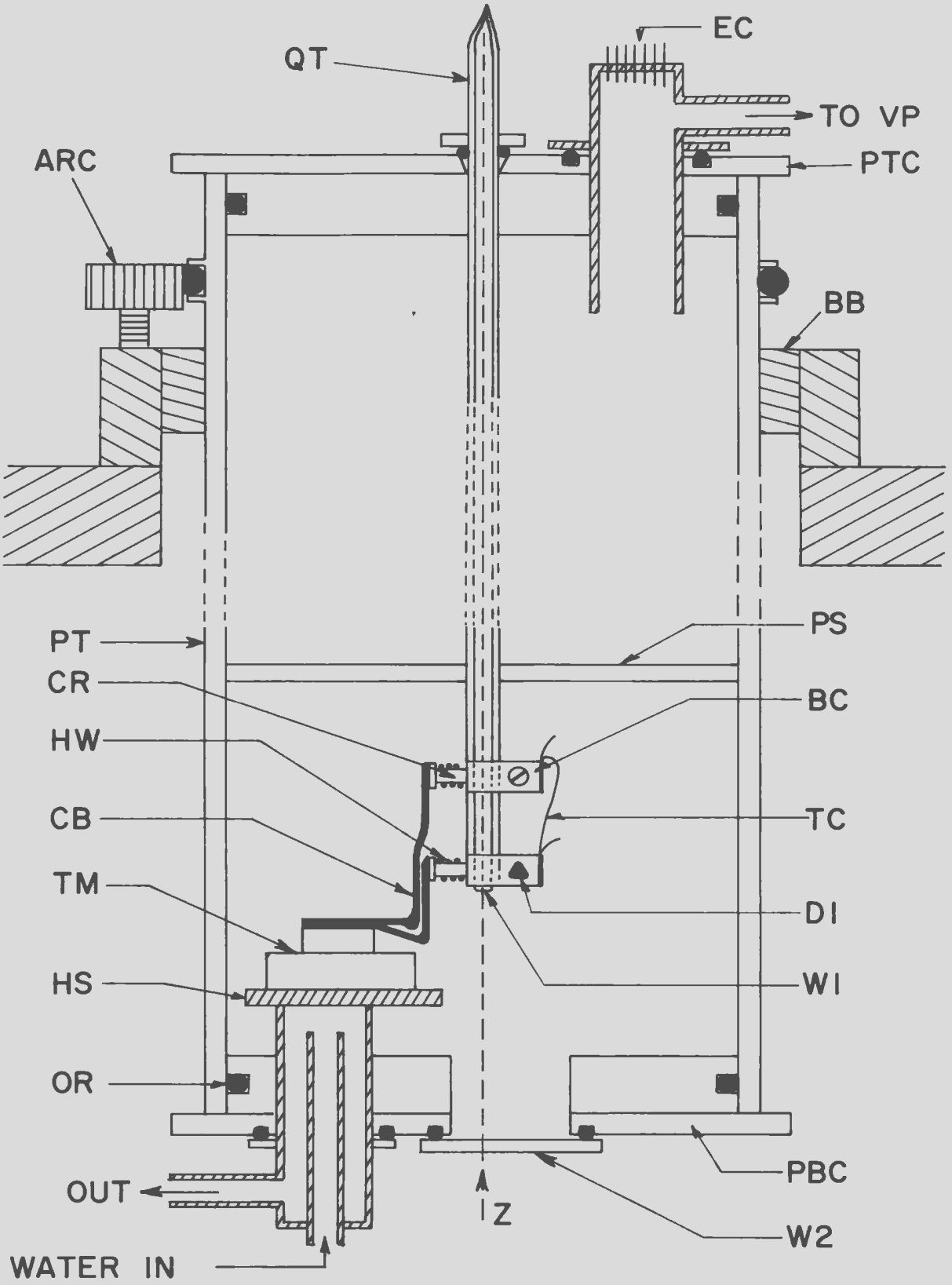
QT
EC
TO VP
PTC
ARC
BB
PT
PS
CR
BC
HW
CB
TC
TM
DI
HS
WI
OR
PBC
OUT
Z
W2
WATER IN

FIGURE 2.2

With reference to Fig. 2.2, a spring clip 5 mm wide and made of brass shim was fastened to the bottom of the cell with a screw-mounted GaAs diode TG-100-T05 (Lake Shore Cryotronics, Inc.). One junction of a (differential) copper-constantan thermocouple was also fastened to this clip near the diode using a good thermal compound. Care was taken that the thermocouple did not make electrical contact with the clip. Another clip was fixed to the cell at a height of about 1 cm above the first clip. The second clip was attached by means of a brass screw, and the other thermocouple juction was fastened to this clip. Copper rods, of 5 mm length and 2 mm diameter, were soldered to each clip, and conducting paths to the thermoelectric cooling element were provided by flexible copper braids attached to the rods. In addition, resistance heaters of $\sim$ 50 ohms were wound on each rod to permit control of the cell temperature.

The cryostat consisted of a plexiglass tube of 8.75 cm inner diameter having 3 mm thick walls. The sample cell was suspended along the central axis of this tube and a plexiglass spacer placed 10 cm from the bottom of the cell ensured that the cell remained along the axis of the tube. The top and bottom of the cryostat were closed with plexiglass covers 1.3 cm thick with the help of a rubber O-ring arrangement so as to make the cryostat vacuum tight. Every other aperture (to be described below) in these covers was also sealed with rubber O-rings.

The bottom cover had a circular aperture whose center was slightly off the axis of the tube. This aperture was closed by a polished fused quartz window (W2) through which the laser beam was

incident along the axis of the sample cell. Another aperture provided a continuous flow of water to a copper heat sink inside the chamber, and the thermoelectric module (described in Section 2.5) which was used to cool the cell was mounted in good thermal contact with the heat sink. The water supply to the heat sink was filtered and the pressure and flow regulated so as to avoid blockage of the tubing and to provide a constant flow of water.

The top cover had a small aperture in the center through which the sample cell passed into the cryostat. A combination of pumping port and electrical feed-through was also provided at the top. Once the whole cryostat was assembled, a vacuum about 2 or 3 μ could easily be maintained inside. This was necessary to avoid thermal convection by air inside the cryostat and consequent uneven gradients along the walls of the sample cell.

The cryostat was supported about 5 cm below its top by means of a ball-bearing arrangement which permitted rotation of the whole cryostat about its (vertical) axis. This rotation could be read to an accuracy of 0.5^{o} via a protractor mounted on top of the cryostat. Thus, Brillouin scattering could be studied at various orientations of the crystal. The ball-bearing sleeve was, in turn, fastened to a flat 2.54 cm thick plate of aluminum by three leveling screws. This plate was equipped with three heavy metal legs and was firmly anchored to a wooden bench which also served as a mounting surface for the optical components.

2.5 Temperature Control and Growth of Single Crystals

It has already been pointed out that the sample cell was cooled by conduction through copper braids. These braids were pressure-bonded to the cold surface of the thermoelectric module as shown in Fig. 2.2. A thermoelectric module is a device which utilizes the Peltier effect to produce a temperature difference between its two surfaces when a direct current is passed through it. The thermoelectric modules used were Module Nos. 12HK and two 8AB8's (Nuclear Systems Inc.). The 8AB8's were mounted on top of 12HK and all of them were connected in series to a power supply (Model 6471, Nuclear Systems Inc.), which was capable of providing variable voltage from 0-6 V dc and a current of up to 6 A. Cooling of the cold surface was proportional to the amount of current passed through the module and also dependent on the temperature of the hot surface. The hot surface of this module was mounted on the heat sink already described (Section 2.4).

To measure the temperature of the crystal and also to keep it at a constant temperature, a cryogenic Temperature Indicator/Controller, Model DTC-500 (Lake Shore Cryotronics, Inc.), was used in conjunction with a GaAs thermometer (Model TG-100K-T05, Lake Shore Cryotronics, Inc.). The GaAs diffused junction thermometer is a diode whose forward voltage changes with temperature when a constant current is passed through it. In the present case, the constant current was 10 microamperes, and the resulting signal ($\sim$ 1V) from the diode was accepted by the temperature controller mentioned above. This signal was compared with a highly stable internal set point voltage; the difference (i.e., the error

signal) was amplified and used to regulate the amount of current flowing through the heaters wound in series around the copper rods supporting the braids. This automatic temperature control was stable to within about 0.01 K per hour.

Apart from playing its part in temperature control, the GaAs diode was also used as a thermometer. The diode was calibrated using constant temperature baths in the range 300 K to 190 K (Meyer 1971) so that, with a current of 10 μA, the voltage developed across the diode was related to the temperature in Kelvins. The output voltage of the diode was equal to the set point voltage when the error signal indicated by the null meter was zero. Thus, by referring this set point voltage to the voltage versus temperature calibration curve, its temperature was obtained. The calibration was accurate to ±0.2 K.

In order to grow a single crystal, it is necessary to maintain a thermal gradient between the top and bottom clips of the cell. This was achieved by dividing the heater current to the top and bottom heaters through a potentiometer connected in parallel with the two heaters. Thus, by adjusting the potentiometer, a thermal gradient of about 1 K was created between the top and the bottom clips. This gradient was constantly monitored by a copper-constantan thermocouple connected to a microvoltmeter (Model 150B, Keithley Instruments). While maintaining the gradient, the temperature of the cell was slowly lowered by adjusting both the current through the thermoelectric module and the set point voltage. When the set point voltage reached the freezing point of cyclohexane, 279.87 K, a small 'seed' crystal about 0.5 mm high was formed. This crystal was annealed for about two to three hours

following which the temperature was slowly lowered so that the crystal grew at an approximate rate of 0.5 mm per hour. When the crystal had grown to about 0.7 cm, further lowering of the temperature was stopped and an X-ray Laue (transmission) photograph was taken. If the crystal appeared to be a completely single crystal and free from any strains and visible defects such as cracks, etc., the temperature and the gradient were kept constant throughout the duration of the experiment. Otherwise, the crystal was melted and another one grown.

CHAPTER 3

EXPERIMENTAL ANALYSIS

3.1 Orientation of Cubic Crystals by X-ray Diffraction

In order to orient the crystal with respect to the laboratory frame of reference, the X-ray Laue diffraction technique was used. Transmission Laue photographs of the sample crystal were taken, firstly, to determine whether the crystal was completely single; secondly, to see if the crystal was strained; and, thirdly, to find the Euler angles (θ,ϕ,χ) (Goldstein 1950) between the crystal axes and the laboratory coordinate axes.

The edges of the cube of phase I of C_6H_{12} were taken to be the major crystalline axes. The laboratory coordinate system and the X-ray apparatus setup is shown in Fig. 2.1. The laser beam was incident along the Z-axis which was also the axis of the cylindrical sample cell. The optical axis (at 90^o to the cell axis) was the Y-axis. During the initial alignment of the apparatus, this optic axis was defined with a He-Ne laser beam. This Y-axis beam intersected the Z-axis beam of the Argon-ion laser at 90^o inside the cylindrical cell about 4 mm from the upper surface of the cell window W1. An accurate pentaprism was used to position the two laser beams.

The X-ray source used was a Philips MO 100/Be 100 Kv beryllium window tube. This is a water-cooled X-ray source and it was operated at 70 Kv and 10 mA current. The X-ray tube was mounted on a very heavy cathetometer with adjustments to provide movements in all directions.

A lead collimator was placed in front of the X-ray source (see Fig. 2.1), followed by the cryostat with the sample cell. The distance between the collimator and the cell was about 4.5 cm. The X-ray beam emerging from the collimator passed through the plexiglass of the cryostat and was incident on the quartz cell containing the crystal. The diameter of this beam was about 1.5 mm, whereas the light scattering volume of the crystal located at the origin of the laboratory coordinates was less than 0.1 mm^3. Thus, the entire volume of the crystal scattering light was probed by the X-rays.

The transmission Laue patterns were recorded using a Polaroid XR-7 Land camera which was mounted between the cell and the spectrometer. The film used was Polaroid, type 57. During the initial alignment, the film surface was placed exactly perpendicular to the Y-axis. The distance between the center of the cell and the surface of the film was 7.0 cm. Once the crystal was grown and probing with the laser beam showed no visible defects (such as cracks in the crystal) a Laue photograph was taken. The Laue pattern consisted of a central bright spot corresponding to the undiffracted beam, and other bright spots produced by the diffraction of X-rays superimposed on a diffuse background (see Fig. 4.1).

In the case of cubic crystals, a relatively strightforward way to analyze the Laue patterns is to use stereographic projection (Cullity 1956). It provides a useful way of showing the three-dimensional relationships among planes and directions in a crystal on a two-dimension graph. A stereographic projection is constructed by considering

a cubic crystal centered in a sphere. From the center, a normal to each face is erected and extended until it meets the sphere in a point. The points and the normals themselves are called 'poles' of the faces. In the (100) standard projection, a line connects the (001) pole of the spherical projection in one-half of the sphere to each pole on the opposite half of the sphere. Then the points where these lines cut the equatorial plane are labelled with the indices of the pole that is connected to (001) and this equatorial plane then forms the stereographic projection.

On the Laue photograph, the distance r of a particular diffraction spot from the center of the film (i.e., the undiffracted spot) is given by (Cullity 1956):

$$r = D \tan 2\theta \tag{3.1}$$

where D = distance between the crystal and the photographic film

2θ = angle between the diffracted and the undiffracted beam.

The distance of the pole of the reflecting plane from the center of the projection is given by

$$r_{pole} = R \tan(45^{o} - \theta/2) \tag{3.2}$$

where R = the radius of the reference sphere, or the radius of the projected great circle.

In analyzing the Laue photographs, a Wulff net of radius R=10 cm was used. Using Eqs. (3.1) and (3.2), a stereographic ruler was

constructed. The spots on the Laue photograph were traced on tracing paper. Then, using this ruler, the poles of the reflecting planes were plotted. The Wulff net was placed below the tracing paper and the angles between the various planes were measured. The crystal orientation was most easily identified if the diffraction pattern exhibited an elliptical pattern of spots characteristic of a crystal zone (i.e., a group of planes parallel to a common line). An example of such a zone can be seen in Fig. 4.1. In this case, all the poles of the zone lie on a great circle of the Wulff net.

The Euler angles (θ,ϕ,χ) were then found by the procedure outlined in Cullity (1956), and were correct to $\pm 2^{o}$. In order to determine the angles to 0.5^{o} accuracy, a computer program was used to plot the Laue spots given by the above Euler angles. These angles were varied by $\pm 1^{o}$ (and later on by $\pm 0.5^{o}$) and all combinations were plotted. Then, by inspection, the computer plot which best fitted the observed spots was taken to be the correct one and the Euler angles corresponding to this plot were taken as accurate to $\pm 0.5^{o}$.

Since the crystal was always rotated about the Z-axis, this meant that only the angle ϕ should change, and θ and χ should remain fixed. However, if the cell was not aligned parallel to the rotation axis, then both θ and χ could change slightly. Such was the case for crystal #1 but, after a modification of the apparatus, the effect was almost entirely eliminated. This was verified by finding the Euler angles corresponding to a number of ϕ rotations of one of the crystals and observing that the variations in θ,χ were within the experimental error.

3.2 Analysis of Spectra

Once the crystal was grown and oriented, a Brillouin spectrum was taken. In a typical scan, usually three full orders of the spectrum were recorded. After the optics had been adjusted for maximum finesse, the drift stabilization and finesse optimization windows were centered on a Rayleigh line of the spectrum. Usually a slight adjustment of lens L2 is necessary to focus on the Brillouin components. Spectra were accumulated in the DAS-1 memory, usually for 30 min to 1 hr, depending upon the intensity of the scattered light, until the various components stood out very clearly above the background noise and were easily measurable. The spectrum was then transferred to the chart paper by the XY-chart recorder.

Actual measurements of the spectra were made directly on the DAS-1 CRT screen using the readout features described in Section 2.3. The Bug was placed on each successive peak of a given spectrum and the channel number as well as the corresponding number of counts in that channel were recorded. Fig. 3.1 shows a stick diagram of a typical spectrum where the Rayleigh (or central) component appears three times and, as in most cases, both the quasilongitudinal and the quasitransverse components appear six times. Once the location of each peak in terms of channel numbers was recorded, the separations ΔL, $\Delta T1$ and $\Delta T2$ were determined and, from these values, the frequency shifts of the various components were calculated as follows:

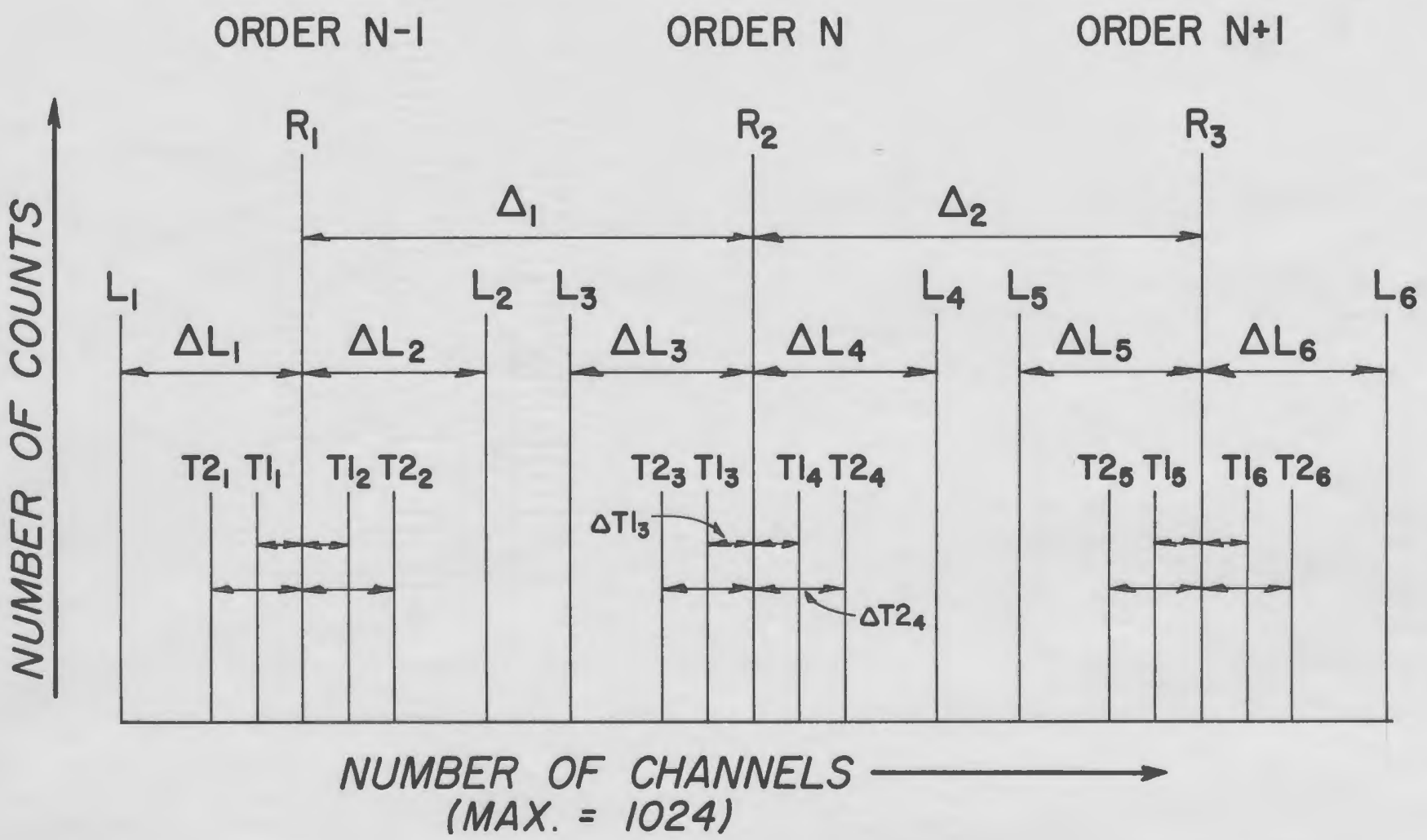

FIGURE 3.1

"Stick-diagram" showing the various measurements made on the spectrum. R's are the Rayleigh components, L's are the longitudinal components and T's the transverse components. Δ, ΔL and ΔT's are used to calculate the frequency shifts of these components.

Spectral free range in channel numbers

$$\Delta = \frac{\Delta_1 + \Delta_2}{2} \tag{3.3}$$

Frequency shifts of longitudinal components

$$\nu(L) = \left(\sum_{i=2}^{5} \Delta L_i \right) \frac{\nu(SFR)}{4\Delta} \tag{3.4}$$

where ν(SFR) is the known value of the spectral free range of the Fabry-Perot in GHz. The frequency shifts of the slow (T1) and fast (T2) quasi-transverse components were calculated in a similar way.

In the above calculations, it was assumed that the frequency scanned by the Fabry-Perot was linearly proportional to the channel numbers of the DAS-1 memory (for one particular order). The difference between Δ_1 and Δ_2 was typically 0.5%. Hence, in the above equations, averaging was done so as to reduce the inaccuracy caused by small non-linearities in the scanning of the interferometer.

3.3 Determination of Elastic Constants

In order to determine the elastic constants of solid cyclohexane near its triple point (6.0°C), the refractive index and density must be known. Density data at various temperatures of solid cyclohexane have been collected by Higgins et al. (1964) and a value of 0.8329 gm cm^{-3} at 6.0°C was determined from their data and their equations given for extrapolation.

No refractive index measurements below the melting point of cyclohexane and at 514.5 nm wavelength were available. Hence, the following procedure was used.

Refractive index measurements for liquid cyclohexane at 25°C and for various wavelengths have been reported by Foss and Schellman (1964). From their data, refractive indices corresponding to wavelengths 365.0, 435.8 and 546.1 nm were used to determine constants A, B, C of the Cauchy relation

$$n = A + \frac{B}{\lambda^2} + \frac{C}{\lambda^4} \quad . \tag{3.5}$$

The refractive index at 25°C and wavelength 514.5 nm was calculated from Eq. (3.5) as

$$n^{25}_{514.5} = 1.4268 \quad . \tag{3.6}$$

The refractive index at 6.0°C was calculated using the Lorentz-Lorenz equation:

$$L(\text{optical})\ \rho = \frac{n^2 - 1}{n^2 + 2} \tag{3.7}$$

where ρ is the density and L(optical) is a constant for a homogeneous, non-polar medium, independent of the density. Hence, using the value of n given by Eq. (3.6) and $\rho = 0.7739$ gm cm^{-3} at 25°C (Forziati et al. 1946), it was calculated that

$$L(\text{optical}) = 0.3316 \quad .$$

Assuming that at 25°C and at 6°C the value of L(optical) remains the same and, using the density at 6°C, the appropriate refractive index was found to be

$$n^{6}_{514.5} = 1.4645 \quad . \tag{3.8}$$

This value of n was used in calculating the elastic constants. The accuracy of this value depends on the assumption that L(optical) remains constant with density changes. (For further discussion on error analysis, see Section 4.3.)

Knowing the values of the incident frequency, the Euler angles, n, ρ, and the Brillouin frequency shifts, further calculations were done on the IBM/370 computer. The programs used for calculating the elastic constants have already been used and perfected by Kiefte and Clouter in their determination of the elastic constants of nitrogen (1976) and oxygen (1975) single crystals.

The scattering wave vector $\vec{K}$ was fixed in the laboratory frame of reference by the scattering configuration equation (1.15), i.e.,

$$\vec{K} = \vec{k}_o - \vec{k} \quad .$$

Since the scattering angle was 90°, then the unit scattering vector has components

$$\hat{K}(\text{LAB}) = (0, K_y, K_z) = (0, 0.7071, -0.7071) \quad . \tag{3.9}$$

The first step in evaluating the elastic constants is to generate a transformation matrix (Goldstein 1950) for each orientation of the crystal

using the Euler angles given in Table 4.2. Then, for each spectrum, $\hat{K}$(LAB) is transformed to $\hat{K}$(CRY) in the crystal frame of reference using this transformation matrix. To determine the elastic constants, first arbitrary values were assumed and then, with the help of Eqs. (1.38) and (1.39),

$$(\lambda_{ij} - \rho\omega^2 \delta_{ij}) \hat{\Pi}_j = 0$$

$$\lambda_{ij} = (C_{11} - C_{44}) K_i^2(\text{CRY}) + C_{44} K^2(\text{CRY}) \quad \text{for } i=j$$

$$= (C_{12} + C_{44}) K_i K_j(\text{CRY}) \quad \text{for } i \neq j$$

the eigenvalues were calculated. In this process, the 3x3 real symmetric matrix λ_{ij} was diagonalized. The diagonal elements give three eigenvalues from which the velocity of that particular mode was calculated from Eq. (1.21):

$$V_\mu(\hat{K}) = \omega_\mu(\vec{K})/|\vec{K}| \quad .$$

The calculated frequency shift was then given by Eq. (1.22) expressed in a different form,

$$\nu_\mu^{\text{calc}} = 2n(V_\mu(\hat{K})/\lambda_o) \sin \theta/2 \quad .$$

This was done for each orientation. The computer program performs a least-squares fit routine starting with the assumed trial values of the elastic constants. Each cycle of iteration produced 28 sets of mode frequencies $\nu_\mu(\vec{K})$ corresponding to the 28 different crystal orientations.

The method of least squares involved minimizing the quantity $\chi(C_{11},C_{12},C_{44})$ with respect to variation of C_{ij}'s:

$$\chi^2(C_{11},C_{12},C_{44}) = \sum_i \left(\frac{\nu_i^{calc}\ (C_{11},C_{12},C_{44}) - \nu_i^{obs}}{\sigma_i} \right)^2 \qquad (3.11)$$

where σ_i is a weighting factor. The sum extends over all 59 shifts used in the determination of elastic constants. The minimization procedure was based on Newton's method and is discussed in detail by McLaren (1973). A weighting factor of one was used for all measurements.

CHAPTER 4

EXPERIMENTAL RESULTS AND DISCUSSION

4.1 Orientation of Cyclohexane Single Crystals

Four single crystals of cyclohexane were successfully grown and oriented for the Brillouin scattering studies. They were 3 mm diameter cylindrical crystals and about 6 mm to 8 mm long. They were clear, colourless, and free from any visible defects. Transmission Laue photographs showed that the four specimens were strain-free single crystals. The temperature controller and the thermoelectric cooler kept the crystals at a constant temperature for days while the experiments were being carried out on them. For each crystal, the temperature in the scattering volume was 279.2 ± 0.2 K. The physical constants of solid cyclohexane are given in Table 4.1.

The procedure for orienting the crystals has already been described in Section 3.1. One point to note is that, when Laue photographs of these crystals were taken, only one or two diffracted spots for most of the orientations were observed. This posed a problem in orienting the crystal as a minimum of three spots is required to calculate the crystal orientation. Except for crystal 4, some particular positions of the crystals were located where more than three spots were obtained in an elliptical pattern (characteristic of a zone). These were then used to orient the crystal. In crystal 4, no orientation was found where more than two spots could be observed. This crystal was oriented by rotating and combining the spots of other orientations into a single picture.

TABLE 4.1

Physical constants of solid cyclohexane

Molecular Weight	84.16 gm $mole^{-1}$	(a)
Triple Point Temperature	279.83 ± 0.01 K	(b)
Triple Point Pressure	39.99 Torr	(c)
Density (279.20 K)	0.8329 gm cm^{-3}	(d)
Refractive Index (279.20 K, wavelength 514.5 nm)	1.4645	(e)
Crystal Structure	fcc (spacegroup T_h^2)	(f)
Lattice Spacing (-5°C)	8.76 Å	(f)
Thermal Expansion Coefficient (Vol.) (at 0°C)	6.26×10^{-4} $^oC^{-1}$	(g)
Entropy of Fusion	9.2 eu	(i)

(a) Handbook of Physics and Chemistry, edited by R. C. Weast (The Chem. Rubber Co., Ohio, 1970-71).

(b) Stokes and Tomlins (1974).

(c) Jackowski, A. W., J. Chem. Therm., 6, 49 (1974).

(d) Higgins et al. (1964).

(e) See Section 3.3.

(f) Hassel and Sommerfeldt (1938); Mitsuo Ito (1965).

(g) Chan and Chew (1969).

(i) Folland et al. (1973).

Fig. 4.1 shows a transmission Laue photograph of crystal 3. Below it is shown the computer-plotted Laue pattern for the Euler angles shown. Each spot is labelled by the Miller indicies of the corresponding set of lattice planes, and the spots actually observed on the photograph are indicated by the solid dots. The black circle in the center of the photograph is a hole in the fluorescent screen of the camera. A shadow cast by the cell is also observed.

Every single spot observed in the Laue photograph was accounted for, and there were no cases where expected spots were not seen. It can be seen in Fig. 4.1 that these (observed) spots arise from planes corresponding to low-order Miller indicies; diffraction from high-order planes was too weak to be recorded on the photographic film. There are several possible reasons why so few Laue spots were observed. The continuous X-ray spectrum is cut off sharply on the short-wavelength side at a value which varies inversely as the tube voltage. This cut-off effect causes higher-order Laue spots for C_6H_{12} to disappear very rapidly towards the center of the film as determined by the Bragg condition. Also, the intensity of the diffracted beam drops sharply with increasing angles of diffraction. This was reported by Hassel and Sommerfeldt (1938) who noted a marked increase in the diffuse nature of the diffraction pattern between $-40^{o}C$ and $-8^{o}C$ because of the considerable increase in the disorder (i.e., increased rotational and translational freedom of movement) with increase in temperature for this plastic crystal.

4.2 Brillouin Scattering Spectrum of Single Crystals of Cyclohexane

Brillouin spectra were recorded for 28 orientations of the four crystals grown. The 514.5 nm light from the Ar-ion laser was incident

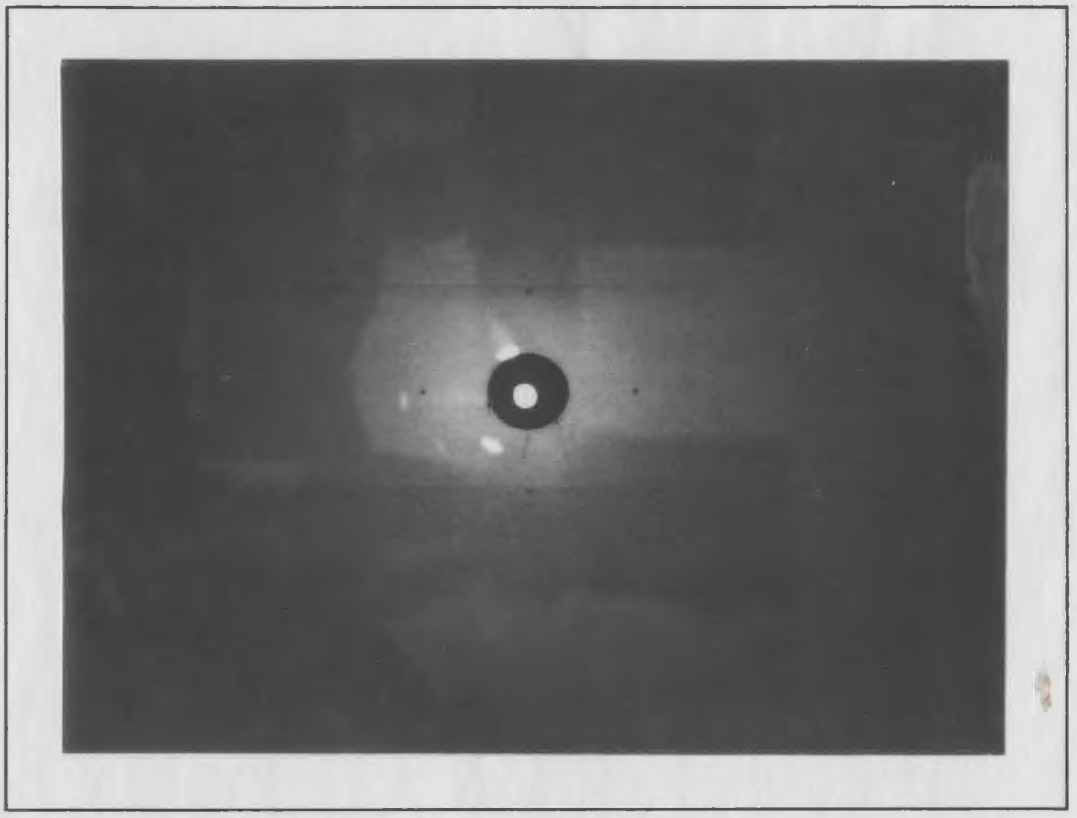

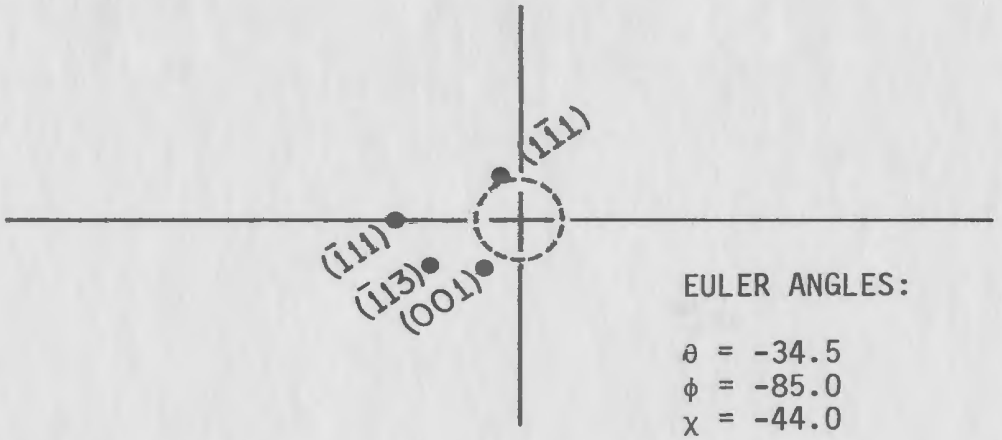

FIGURE 4.1

The transmission Laue photograph of crystal 3 at a particular orientation. Below is shown the computer-plotted Laue pattern and the corresponding Euler angles. The spots are labelled with the Miller indices of the reflecting planes.

along the cell axis (Z-axis) and was polarized in the X-direction. The spectrometer measured the total intensity scattered in the Y-direction (scattering angle was $90^{o} \pm 0.5^{o}$).

An example of a spectrum is shown in Fig. 4.2. This was recorded for crystal 3 at $\theta = -34.5$, $\phi = -28.0$, and $\chi = -44.0$. As discussed in Section 1.4, in crystalline solids, three Brillouin components should be observed. However, in only three of the 28 spectra were all three components present. In crystals 1 and 3, L (quasi-longitudinal) and T1 (slow-quasitransverse) components were observed, whereas in crystal 2, L and T2 (fast-quasitransverse) components were present. In crystal 4 at three particular orientations (as given in Table 4.2), all three components were present; in one orientation, L and T2 were present, and in the rest L and T1 were present. The intensity of the central unshifted component is about two to five times as much as the L component. It is believed that the central component is mostly due to parasitic scattering. Its intensity could not be reduced, but it did not seriously affect the Brillouin spectrum because of the high finesse of the Fabry-Perot spectrometer. It was found that the L components were very intense compared to the T1 and T2 components, and also the slow-quasitransverse component T1 was usually slightly more intense than the fast-quasitransverse component T2. It was also observed that, when the incident electric field, $\vec{E}$, was polarized in the scattering plane (i.e., Y-Z plane)

FIGURE 4.2

Brillouin spectrum of crystal 3 at the orientation specified by the Euler angles (θ,ϕ,χ). Only one complete order has been shown. The spectrum was scanned 1575 times at a rate of 2 ms per channel which corresponds to 2.2×10^4 counts/sec at the center channel of the Rayleigh peak. The incident radiation was polarized perpendicular to the scattering plane.

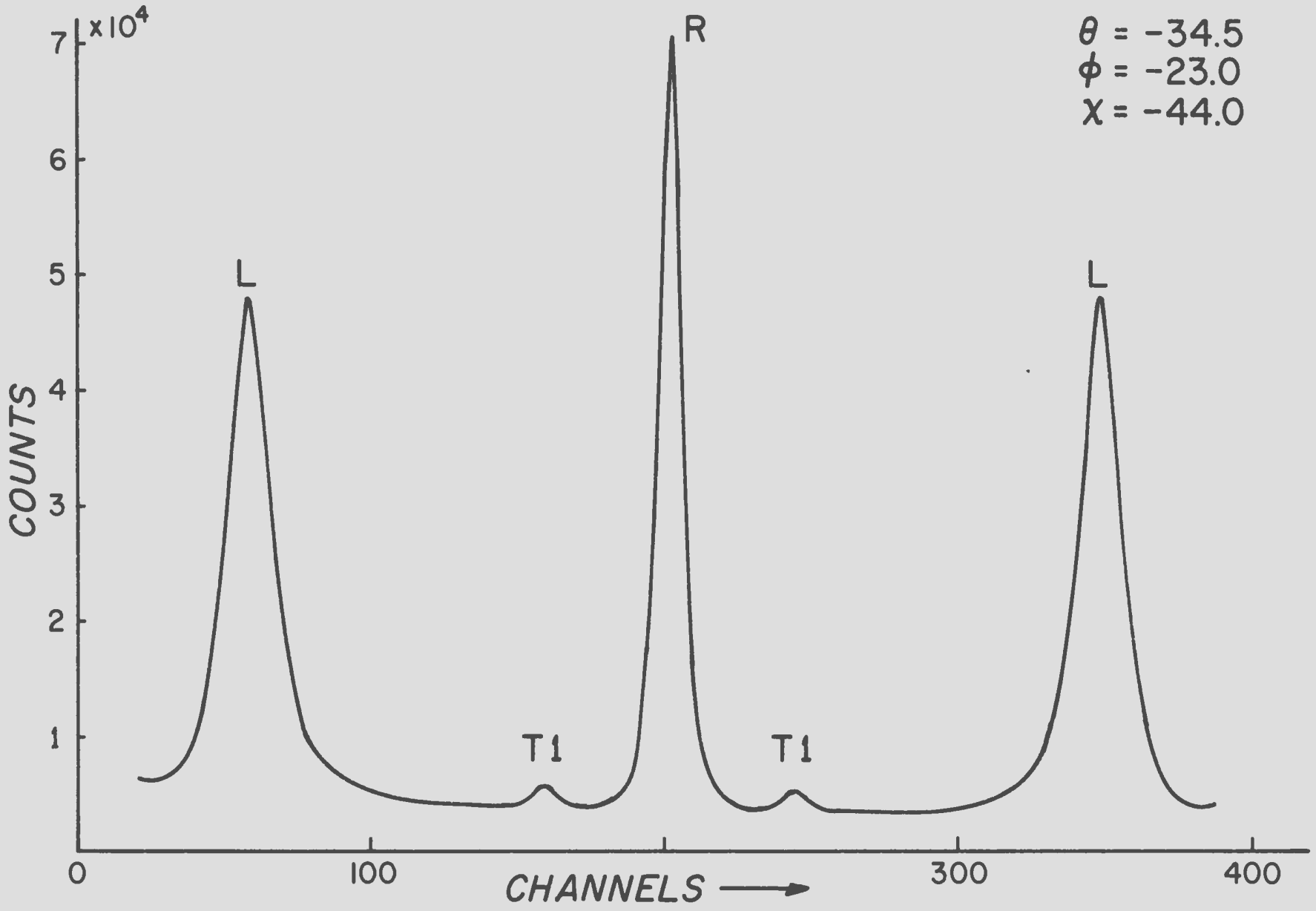
x10^4
7
6
5
4
3
2
1
COUNTS
L
R
L
T1
T1
θ = -34.5
φ = -23.0
χ = -44.0
0
100
300
400
CHANNELS

FIGURE 4.2

TABLE 4.2

Observed and calculated Brillouin shifts as a function of orientation for four cyclohexane single crystals, at 279.2 ± 0.2 K

CRYSTAL	Euler angles in degrees θ	ϕ	χ	Observed frequency shifts in GHz ν(L)	ν(T2)	ν(T1)	Calculated frequency shifts in GHz ν(L)	ν(T2)	ν(T1)
1	-141.0	-85.0	-28.5	7.63	—	2.06	7.648	2.637	2.008
	-141.0	-79.0	-28.5	7.68	—	1.99	7.660	2.636	1.965
	-141.0	-39.5	-28.5	7.60	—	2.20	7.602	2.571	2.256
	-141.0	-29.5	-28.5	7.55	—	2.35	7.553	2.577	2.408
2	-9.0	14.0	8.5	7.69	2.46	—	7.688	2.496	2.036
	-9.0	24.0	8.5	7.73	2.37	—	7.714	2.385	2.070
	-9.0	35.0	8.5	7.73	2.25	—	7.733	2.267	2.134
	-9.0	46.0	8.5	7.70	2.30	—	7.734	2.255	2.142
	-9.0	56.0	8.5	7.70	2.37	—	7.720	2.368	2.069
	-9.0	66.0	8.5	7.71	2.51	—	7.699	2.487	2.008
	-9.0	76.0	8.5	7.67	2.58	—	7.679	2.582	1.963
3	-34.5	-85.0	-44.0	7.65	—	2.03	7.651	2.588	2.062
	-34.5	-70.0	-44.0	7.62	—	2.18	7.594	2.636	2.205
	-34.5	-60.0	-44.0	7.56	—	2.30	7.569	2.628	2.301
	-34.5	-48.0	-44.0	7.58	—	2.41	7.565	2.570	2.376
	-34.5	-38.0	-44.0	7.61	—	2.35	7.586	2.536	2.347
	-34.5	-28.0	-44.0	7.60	—	2.26	7.620	2.548	2.221

TABLE 4.2 (Continued)

CRYSTAL	Euler angles in degrees			Observed frequency shifts in GHz			Calculated frequency shifts in GHz		
	θ	ϕ	χ	ν(L)	ν(T2)	ν(T1)	ν(L)	ν(T2)	ν(T1)
3	-34.5	-18.0	-44.0	7.63	—	2.06	7.654	2.565	2.080
	-34.5	-8.0	-44.0	7.65	—	1.96	7.676	2.575	1.983
4	-119.0	84.0	4.0	7.71	2.36	—	7.706	2.381	2.107
	-119.0	94.0	4.0	7.70	2.53	2.08	7.692	2.483	2.039
	-119.0	104.0	4.0	7.69	2.59	1.98	7.680	2.570	1.975
	-119.0	114.0	4.0	7.67	2.69	1.90	7.671	2.622	1.942
	-119.0	124.0	4.0	7.66	—	1.96	7.661	2.638	1.959
	-119.0	134.0	4.0	7.65	—	2.09	7.646	2.624	2.034
	-119.0	144.0	4.0	7.64	—	2.14	7.623	2.593	2.156
	-119.0	154.0	4.0	7.60	—	2.27	7.593	2.561	2.297
	-119.0	164.0	4.0	7.57	—	2.37	7.560	2.557	2.408

the intensity of the longitudinal components decreased as compared to the case when $\vec{E}$ was polarized perpendicular to the scattering plane (i.e., in X-Z plane).

Table 4.2 contains the crystal orientation in terms of Euler angles and the observed and calculated Brillouin shifts. The latter were obtained from the "best-fit" elastic constants. It can be seen that, for different orientations of the crystal, the frequency of the components changes.

4.3 Elastic Constants and Error Analysis

The procedure for the determination of elastic constants of cyclohexane single crystals from the measured Brillouin shifts has already been outlined in Section 3.3

All four crystals were studied at the same temperature (279.2 $\pm$ 0.2 K). The data from all of them were, therefore, combined to determine the "best-fit" values of the elastic constants which are given in the first row of Table 4.3. The relative values are estimated to be accurate to 1%. Since two different samples of cyclohexane were used to grow the crystals, a check could be performed on the internal consistency of the results, i.e., to see whether the two samples gave different values of the elastic constants. The elastic constants were evaluated first by using the data of crystals 1 and 2 of sample A, and then by using the data of crystals 3 and 4 of sample B. As seen in Table 4.3, the values so obtained agree with each other and with the "best" values.

TABLE 4.3

Adiabatic elastic constants of solid cyclohexane,

at 279.2 ± 0.2 K

(in units of 10^9 N m^{-2})

	N*	C_{11}	C_{12}	C_{44}
All 4 crystals	59	2.8(57)	2.4(72)	0.35(8)
Sample A[1]				
Crystal 1	8**			
Crystal 2	14			
Crystals 1 and 2	22	2.8(72)	2.4(72)	0.3(49)
Sample B[2]				
Crystal 3	16			
Crystal 4	21			
Crystals 3 and 4	37	2.8(52)	2.4(72)	0.3(64)

*N is the number of Brillouin shifts included in each determination.

[1]Sample A is the cyclohexane obtained from J. T. Baker Chem Co. (GC-Spectrophotometric quality).

**Unfortunately, crystal 1 was destroyed because of power failure, before which only four spectra were recorded.

[2]Sample B is the cyclohexane obtained from Anachemia Chem Ltd. (Suitable for U.V. spectrophotometry, 99.98%).

The uncertainty of 1% for the elastic constants given in Table 4.3 arises essentially from a combination of the uncertainties in the measurements of the Brillouin shifts and the crystal orientation determinations. The measurement uncertainty depends basically on the accuracy with which the peaks can be estimated and located, the frequency shifts that can be measured on the DAS-1 CRT screen, and the linearity in the scanning of the Fabry-Perot. The orientation uncertainty is the possible error in the determination of the Euler angles. Note that (in Table 4.2) all measured shifts were individually fit to well within 2.5%.

Additional uncertainties in the constants result from possible errors in the wavelength, spectral free range ν(SFR), density ρ refractive index n, and the scattering angle. The errors in these quantities will change the absolute values of the elastic constants by the same factor. The wavelength was considered exact (10^{-5}% uncertainty), and the uncertainty in ν(SFR) is 0.1%. The uncertainty in ρ is reported to be 0.05% (Higgins et al. 1964), while the uncertainty in n depends on the accuracy of the Lorentz-Lorenz constant L(optical) (see Section 3.2) and ρ. The uncertainty in L(optical) was estimated as follows. The dielectric measurements (Chan and Chew 1969) and the density measurements of liquid and solid C_6H_{12} (Higgins et al. 1964; and Forziati et al. 1946) were used to calculate the value of L(static) from the Clausius-Mossotti equation

$$\frac{\varepsilon-1}{\varepsilon+2} = \rho L(\text{static}) \quad .$$

It was found that the value of L(static) changes by about 3% just near the triple point (279.83 K); otherwise, below the triple point (from 277 K to 237 K) and above the triple point (from 281 K to 298 K) it remains fairly constant to within 0.5%. The dielectric constant changes so rapidly with temperature at the triple point that most of the uncertainty arises mainly from this data. With the above argument in mind, it was assumed that the uncertainty in L(optical) in the Lorentz-Lorenz relation (Eq. 3.7) could be as large as the change in L(static), i.e., approximately 3%. Hence, the uncertainty in n is estimated to be about 1%.

The uncertainty in the scattering angle results from the fact that the angle was possibly not precisely 90^{o}. Also, the axis of the cell was possibly not strictly perpendicular, with the result that there would have been some deviation of the light coming out of the cylindrical cell, thus further changing the scattering angle. It was estimated that the resulting scattering angle was $90^{o} \pm 0.5^{o}$. When all these factors are combined, the additional uncertainty is about 1.2%. These were added to the relative "best-fit" (1%) uncertainties in the elastic constants.

Hence, the final results for the adiabatic elastic constants of solid cyclohexane at 279.2 ± 0.2 K are as follows (in units of 10^{9} N m^{-2}):

$$C_{11} = 2.8(57)$$

$$C_{12} = 2.4(72)$$

$$C_{44} = 0.35(8)$$

correct to within 2%, taking into account all the experimental errors. It should be noted that this is the error in the absolute values of the elastic constants; the error in the ratios of these constants is estimated to be less than 1%.

The elastic anisotropy A, the adiabatic bulk modulus B_s and the shear modulus G are:

$$A = 2C_{44}/(C_{11}-C_{12}) = 1.86$$

$$B_s = (C_{11} + 2C_{12})/3 = 2.60 \times 10^9 \text{ N m}^{-2}$$

$$G = (C_{11} - C_{12})/2 = 0.19 \times 10^9 \text{ N m}^{-2}$$

The estimated uncertainty in B_s is 3%, in A is 10%, and in G is 20%.

The velocities of elastic waves in the principal symmetry directions of a single crystal of cyclohexane can be determined (Kittel 1971) using the elastic constants. The velocities calculated for the three (pure) modes are given below in m sec^{-1}:

	<100>	<110>	<111>
Longitudinal L	1852	1905	1923
Fast-transverse T2	657	657	546
Slow-transverse T1	657	481	546

4.4 Discussion

This is the first known study where Brillouin spectroscopy has been used to determine the adiabatic elastic constants of single crystals of cyclohexane near the triple point. The only other known attempt to

determine the adiabatic elastic constants of cyclohexane in the temperature range -20°C to -80°C was done by Scheie (1965) using the ultrasonic (transit-time) technique. He measured transverse and longitudinal velocities on *polycrystalline* samples. Then, by assuming the Cauchy condition for isotropic and cubic crystals, viz.,

$$C_{12} \simeq C_{44} \quad ,$$

he has calculated adiabatic elastic constants for *single* crystals by mathematical and graphical arguments. However, as the present results show,

$$C_{12} \simeq 7\, C_{44} \quad ,$$

hence, the Cauchy condition does not hold for single crystals of cyclohexane near the triple point. (This means that the intermolecular forces are not central in nature.) Consequently, it can be assumed that the Cauchy condition will not hold at -86°C, where the plastic phase changes into a non-plastic phase.

Because of the drastic assumption made, the values of the adiabatic elastic constants as determined by Scheie (1965), and Green and Scheie (1967), when extrapolated to the triple point do not agree at all with the present results. In fact, their values are very low, apart from the fact that $C_{12} \neq C_{44}$. However, it may well be that the ultrasonic adiabatic elastic constants are different from the hypersonic elastic constants.

It is interesting to compare the Brillouin spectrum and the elastic constants of other molecular plastic crystals. Table 4.4 gives

TABLE 4.4

Comparative elastic data of some plastic and rare-gas crystals

Substance	Crystal structure	Temperature in K*	Adiabatic elastic constants in 10^9 N m^{-2}					Elastic anisotropy A	Adiabatic bulk modulus in 10^9 N m^{-2}	C_{12}/C_{44}**
			C_{11}	C_{12}	C_{44}	C_{13}	C_{33}			
Cyclohexane	fcc	279.2	2.857	2.472	0.358	–	–	1.86	2.60	6.9
Succinonitrile[1]	bcc	–	5.07	3.54	0.65	–	–	0.85	4.05	5.5
Pivalic acid[2]	fcc	298.2	3.304	1.456	0.642	–	–	0.69	2.07	2.3
Norbornylene[3]	hex	296.0	4.01	3.59	0.91	3.00	4.01	4.33	3.73	3.3
γ-Oxygen[4]	fcc	54.2	2.598	2.058	0.275	–	–	1.02	2.24	7.5
β-Nitrogen[5]	hex	63.0	1.825	1.131	0.320	0.980	1.976	0.92	1.31	3.1
Xenon[6]	fcc	156.0	2.98	1.90	1.48	–	–	2.74	2.26	1.3
Krypton[7]	fcc	115.6	2.657	1.725	1.261	–	–	2.71	2.04	1.4
Argon[8]	fcc	82.0	2.33	1.49	1.17	–	–	2.80	1.77	1.3
Neon[9]	fcc	24.3	1.18	0.74	0.60	–	–	2.74	0.89	1.2

TABLE 4.4 (Continued)

*Temperature at which elastic constants are evaluated.

**For hexagonal crystals, the relevant ratio is C_{13}/C_{44}.

[1]Fontain and Moriamez 1968, ultrasonic measurements.

[2]Bird et al. 1973.

[3]Folland et al. 1975.

[4,5]Kiefte and Clouter 1975, 1976.

[6]Gornall and Stoicheff 1971.

[7]Jackson et al. 1973.

[8]Gewurtz et al. 1972.

[9]McLaren et al. 1974.

the values of elastic constants and other data of some plastic and non-plastic crystals. It can be seen that the adiabatic elastic constants of C_6H_{12} are of the same order of magnitude as molecular plastic crystals, viz., succinonitrile, pivalic acid and norbornylene. However, the magnitude of the elastic constants of cyclohexane are lower than the above three plastic-solids (except C_{12} of pivalic acid). This shows that the intermolecular forces (Van der Waal forces) in C_6H_{12} are weaker. In the above-named solids, only one transverse component has been observed. In succinonitrile at lower temperatures, not even one transverse component is observed, i.e., at temperatures below 290 K. Recently, a Brillouin scattering experiment on another plastic single crystal of CBr_4 (Tekippe et al. 1977) shows two transverse components. Unfortunately, the crystal was not oriented and, hence, the elastic constants are not available for comparison. In cyclohexane in crystal 4, both transverse components were observed at three different orientations of the crystals. The intensity of the slow-quasitransverse component is about ten times smaller than the intensity of quasilongitudinal components in cyclohexane which is similar to that in norbornylene and pivalic acid. In CBr_4, the slow quasitransverse components seem to be a bit stronger but the fast quasitransverse component appears to be weak.

The bulk modulus B_s of cyclohexane is comparable to that of pivalic acid; however, the order of magnitude of B_s of succinonitrile and norbornylene is the same. In C_6H_{12}, the elastic anisotropy A is greater than unity (1.86), whereas, in succinonitrile and pivalic acid, it is less than unity. This means that the nature of the anisotropy is

reversed in cyclohexane, as a consequence of which the longitudinal mode hypersonic velocity is greatest in the <111> direction in C_6H_{12}, whereas it will be greatest in the <100> direction for the other two plastic solids.

It is worth noting that none of the above plastic crystals satisfies the Cauchy conditions, as can be seen in the last column of Table 4.4.

Plastic crystals of diatomic molecules provide a striking comparison. The elastic constants of γ-oxygen and β-nitrogen single crystals are of the same order of magnitude as cyclohexane. γ-oxygen is more similar to C_6H_{12} in that the elastic constants, the bulk modulus and the disagreement with the Cauchy condition are roughly of the same magnitude in both. Both γ-oxygen and C_6H_{12} are plastic crystals and have an fcc crystal structure in this phase. The dissimilarity between the two is that γ-oxygen is highly isotropic (elastic) at its melting point, whereas cyclohexane is somewhat anisotropic. Similarly, β-nitrogen plastic single crystals are also fairly isotropic and do not satisfy the Cauchy condition. Because of its high isotropic character, only one transverse component was observed in γ-oxygen, and the intensity of the transverse components is comparable to the longitudinal components which is a unique feature so far unobserved in other plastic or any molecular crystals.

In monatomic rare-gas single crystals, the C_{11}'s are roughly of the same magnitude as that of cyclohexane (except neon), whereas C_{12}'s are lower and C_{44}'s are of higher value. The anisotropy of rare-gas crystals is high but they approximately obey the Cauchy condition.

Brillouin scattering experiments on non-plastic molecular crystals have not been done extensively. However, such an experiment is reported for single crystals of s-trichlorobenzene (Swanson et al. 1974). As expected, the elastic constants of this crystal are much higher than those of cyclohexane and, in general, are higher than those of other plastic crystals. Similarly, it should be noted that the elastic constants of molecular plastic crystals and rare-gas crystals are, in general, one to two orders of magnitude smaller than those associated with non-plastic molecular, ionic or metallic crystals.

The elastic constants given in Section 4.3 were calculated just below the triple point. The positions of the quasitransverse and quasi-longitudinal components extremely close to and at the triple point were also investigated. The possible merging together of the two quasi-transverse components was studied in particular detail as the triple point was approached very closely. Crystal 4 at orientation (-119.0, 104.0, 4.0) was selected (because of the appearance of two transverse components). The crystal temperature was raised slowly and spectra were taken at every 0.05 K rise of temperature until, at the triple point, the liquid-solid interface was probed where not only the two transverse components were present but also longitudinal components of both the liquid state and the plastic phase. The longitudinal frequency shift of the liquid state was less than that of the solid phase. First of all, it is clear that at the phase transition there is a distinct jump in the longitudinal frequency shifts which is much more than can be accounted for by considering the changes in the refractive index only.

This is in contradiction to the ultrasonic measurements of Green and Scheie (1967) where the longitudinal components in the liquid phase and in the plastic phase at the triple point were found to have the same velocity. A similar jump in the longitudinal velocity has been found in the case of single crystals of CBr_4 (Tekippe et al. 1977) and in polycrystaline CCl_4 (Levy-Mannheim et al. 1974). Secondly, the two transverse components do not merge together and then the phase transformation destroys them completely. Hence, it can be concluded that the elastic constants obtained are valid at the triple point of cyclohexane and, in particular, that the crystal remains elastically anisotropic right up to the phase transition.

Studies of the temperature dependence of the elastic constants of cyclohexane and especially the determination of these values at the solid-solid transformation point at $-86^{o}C$ will be initiated shortly.

REFERENCES

Andrew, E. R. and R. G. Eades, Proc. Roy. Soc., A216, 398 (1953).

Benckert, L. and G. Backstrom. Phys. Rev. B, 8, 5888 (1973).

Benedek, G. B. and K. Fritsch, Phys. Rev., 149, 647 (1966).

Bird, M. J., D. A. Jackson and H. T. A. Pentecost, in: Proceedings of the Second International Conference on Light Scattering in Solids, edited by M. Balkanski (Flammarion Sciences, Paris, 1971), p. 493.

Bird, M. J., D. A. Jackson and T. G. Powles, Molecular Phys., 25, 1051 (1973).

Borcherds, P. H., Optica Acta, 20, 147 (1973).

Born, M. and K. Huang, Dynamical Theory of Crystal Lattices (Clarendon Press, Oxford, 1954).

Boyer, L., R. Vacher, M. Adam and L. Cecchi, in: Proceedings of the Second International Conference on Light Scattering in Solids, edited by M. Balkanski (Flammarion Sciences, Paris, 1971), p. 498.

Brillouin, L., Ann. Phys. (Paris), 17, 88 (1922).

Carpenter, G. B. and R. S. Halford, J. Chem. Phys., 15, 99 (1947).

Chan, R. K. and H. A. Chew, Can. J. Chem., 47, 2249 (1969).

Chiao, R. Y. and B. P. Stoicheff, J. Opt. Soc. Amer., 54, 1286 (1964).

Clouter, M. J. and H. Kiefte, J. Chem. Phys., 59, 2537 (1973).

Clouter, M. J., H. Kiefte and C. W. Cho, Solid. St. Comm., 14, 579 (1974).

Clouter, M. J., H. Kiefte and I. E. Morgan, Can. J. Phys., 53, 1727 (1975).

Cullity, B. D., Elements of X-ray Diffraction (Addison-Wesley, Reading, Ma., 1956).

Cummins, H. Z. and P. E. Schoen: Laser Handbook, Vol. 2, edited by F. T. Arecchi and E. O. Schulz-dubois, pp. 1030-75 (North-Holland Co., Amsterdam, 1972).

Dobromyslov, N. A., N. I. Koshkin and V. H. Suvorov, Zh. Fiz. Khim., 48, 2208 (1974). English Trans.: Russ. J. Phys. Chem., 48, 1308 (1974).

Dows, D. A., J. Mol. Spect., 16, 302 (1965).

Dunning, W. J., Phys. and Chem. Solids, 18, 21 (1961).

Durand, G. E. and A. S. Pine, IEEE J. Quant. Elect., QE-4, 523 (1968).

Fabelinskii, I. L., Soviet Phys. Usp., 5, 667 (1963).

Fabelinskii, I. L., Molecular Scattering of Light, Translated by R. T. Beyer (Plenum Press, New York, 1968).

Fleury, P. A. and J. P. Boon, Phys. Rev., 186, 244 (1969).

Folland, R., S. M. Ross and J. H. Strange, Mol. Phys., 26, 27 (1973).

Folland, R., D. A. Jackson and S. Rajagopal, Mol. Phys., 30, 1053 (1975).

Fontaine, H. and C. Moriamez, J. Chimie Phys., 65, 969 (1968).

Forziati, A. F., A. R. Glasgow, Jr., C. B. Williamham and F. D. Rossini, J. Res. Natl. Bur. Stds., 36, 129 (1946).

Foss, J. G. and J. A. Schellman, J. Chem. Engg. Data, 9, 551 (1964).

Gewurtz, S., H. Kiefte, D. Landheer, R. A. McLaren and B. P. Stoicheff, Phys. Rev. Lett., 29, 1454 (1972).

Gilbert, M. and M. Drifford, J. Chem. Phys., 66, 3205 (1977).

Goldstein, H., Classical Mechanics (Addison-Wesley, Cambridge, 1950), p. 107.

Gorbunov, M. A., N. I. Koshkin and D. V. Sheloput, Soviet Phys. - Acoustics, 12, 20 (1966).

Gornall, W. S., Ph.D. Thesis, University of Toronto, 1970 (unpublished).

Gornall, W. S. and B. P. Stoicheff, Phys. Rev. B, 4, 4518 (1971).

Green, J. R. and C. E. Scheie, J. Phys. Chem. Solids, 28, 383 (1967).

Greytak, T. J. and G. B. Benedek, Phys. Rev. Lett., 17, 179 (1966).

Grimsditch, M. H. and A. K. Ramdas, Phys. Rev. B, 11, 3139 (1975).

Gross, E., Nature, 126, 201 (1930).

Hassel, O. and A. M. Sommerfeldt, Z. Physik. Chem., B40, 391 (1938).

Hawthorne, H. M. and J. N. Sherwood, Trans. Faraday Soc., 66, 1783 (1970).

Hayes, W., Comtemp. Phys., 16, 69 (1975).

Higgins, P. F., R. A. B. Ivor, L. A. K. Staveley and J. J. des C. Virden, J. Chem. Soc., Suppl. No. 1, 5762 (1964).

Ito, Mitsuo, Spectrochimica Acta, 21, 2063 (1965).

Jackson, J. D., Classical Electrodynamics (John Wiley and Sons, Inc., N.Y., 1962, 1st Edition), p. 119.

Jackson, H. E., D. Landheer and B. P. Stoicheff, Phys. Rev. Lett., 31, 296 (1973).

Kiefte, H. and M. J. Clouter, J. Chem. Phys., 63, 3863 (1975).

Kiefte, H. and M. J. Clouter, J. Chem. Phys., 64, 1816 (1976).

Kittel, C., Introduction to Solid State Physics (John Wiley and Sons, Inc., N.Y., 1971, 4th Edition).

Koshkin, N. I. and N. A. Dobromyslav, Russ. J. Phys. Chem., 44, 724 (1970).

Krishna Murti, G. S. R., Ind. J. Phys., 32, 460 (1958).

Krishnan, R. S., Proc. Indian Acad. Sci., A41, 91 (1955).

Levy-Mannheim, C., M. Djabourov, J. Leblond and P. H. E. Meijer, Phys. Lett., 50A, 75 (1974).

McLaren, R. A., Ph.D. Thesis, University of Toronto, 1973 (Unpublished).

McLaren, R. A., H. Kiefte, D. Landheer and B. P. Stoicheff, Phys. Rev. B, 11, 1705 (1975).

Meyer, B., Low Temperature Spectroscopy (American Elsevier Pub. Co., N.Y., 1971), p. 220.

Morgan, I. E., M.Sc. Thesis, Memorial University of Newfoundland, 1976 (Unpublished).

Quate, C. F., C. D. W. Wilkinson and D. K. Winslow, Proc. IEEE, 53, 1604 (1965).

Rasmussen, R. A., J. Chem. Phys., 36, 1821 (1962).

Rawson, E. G., E. H. Hara, A. D. May and H. L. Welsh, J. Opt. Soc. Amer., 56, 1403 (1966).

Rytov, S. M., Soviet Phys. JETP, 6, 401 (1958).

Scheie, C. E., Ph.D. Thesis, University of New Mexico, 1965 (Unpublished).

Shapiro, S. M., R. W. Gammon and H. Z. Cummins, Appl. Phys. Lett., 9, 157 (1966).

Smith, R. A., Contemp. Phys., 12, 523 (1971).

Stokes, R. H. and R. P. Tomlins, J. Chem. Thermod., 6, 379 (1974).

Swanson, D. L. and D. A. Dows, Chem. Phys. Lett., 23, 430 (1973).

Swanson, D., L. C. Brunel and D. A. Dows, J. Chem. Phys., 63, 3863 (1975).

Tekippe, V. J. and L. L. Abels, Phys. Lett., 60, 129 (1977).

Timmermans, J., Les Constantes Physiques des Composes Organiques Cristalles (Masson, Paris, 1953).